MASTERARBEIT | MASTER'S THESIS

Titel | Title

Cellular composition at the fetal-maternal interface of Guinea Pig

verfasst von | submitted by

Eyleen Engel BSc

angestrebter akademischer Grad | in partial fulfilment of the requirements for the degree of

Master of Science (MSc)

Wien | Vienna, 2024

Studienkennzahl lt. Studienblatt | Degree programme code as it appears on the student record sheet:	UA 066 831
Studienrichtung lt. Studienblatt | Degree programme as it appears on the student record sheet:	Masterstudium Zoologie
Betreut von | Supervisor:	Univ.-Prof. Mag. Dr. Mihaela Pavlicev

Acknowledgements

I wish to express my sincere gratitude to Mihaela Pavličev for introducing me to the world of reproductive biology and welcoming me into her project. I am also thankful to Silvia Basanta for sharing invaluable insights into guinea pig research, and to Gülay Dagdas for her assistance in the lab and unwavering support. My heartfelt appreciation goes to the entire Pavličev group for their time, encouragement, and actual support throughout my master thesis.

Furthermore, my family deserves my whole-hearted appreciation for their support, both financially and emotionally, throughout my entire studies. At last, I wish to thank my partner for bringing moments of laughter and happiness into my writing breaks, making the journey all the more enjoyable.

Table of Contents

1. Abstract

Reproductive success is key for the continuity of populations, the persistence of biological systems and their evolution. In eutherians, a functional extra-embryonic tissue and its interaction with maternal tissues contributes significantly to the development of a healthy embryo, and thus the reproductive success. While the placenta and its variability across eutherians is well appreciated, little attention has been paid to extra-placental and maternal tissue involved in the fetal-maternal interface. Deciphering the interaction of these components provides insight into the mechanisms and processes that underpin a healthy pregnancy. While broader comparative work is necessary to gain an understanding of this aspect in pregnancy, the present contribution focuses on the fetal-maternal interface in guinea pig (*Cavia porcellus*). We investigate the cell composition of the interface at three time points of the long gestation (6.5, 30.5, and 55 days post copulation) and at the non-pregnant stage in diestrus. In doing so, we utilize histological staining methods to generate a gross description on the morphology and cell types present within the reproductive tissue of guinea pigs. Additionally, we compare the findings with newly generated single-cell RNA sequencing data generated by Basanta & Stadtmauer (in prep.). We observed the most significant diversification of the cells at the fetal-maternal interface between the time point of implantation (6.5 dpc) and the mid gestational time point (30.5 dpc). This period comprises crucial processes such as decidualization of the endometrium and the formation of placental structures, shaping the guinea pig utero-placental interface. These include the accessory subplacenta, a structure resembling the villi of the human chorio-allantoic placenta. In the second portion of pregnancy, after the luteo-placental shift in progesterone production, the processes of degeneration set in. These include the eventual loss of the subplacenta and the accumulation of amorphous dead cell masses in the broad junctional zone. This junctional zone separates placental tissue from maternal decidua and exhibits a chaotic appearance characteristic of this species. These findings shed light on the complexity of the process leading to the establishment of the utero-placental interface and its transformation throughout the guinea pig's pregnancy.

2. Zusammenfassung

Reproduktiver Erfolg ist von entscheidender Bedeutung für das Fortbestehen von Populationen, die Stabilität von biologischen Systemen und die Evolution insgesamt. Bei Eutheria trägt ein funktionelles extraembryonales Gewebe und dessen Interaktion mit maternalem Gewebe wesentlich zur Entwicklung eines gesunden Embryos und somit zum reproduktiven Erfolg bei. Während die Plazenta und ihre Variabilität innerhalb der Eutheria anerkannt sind, wurde wenig Aufmerksamkeit auf das extra-plazentale und maternale Gewebe gerichtet, welches an der fötal-maternalen Verbindungsschicht beteiligt ist. Die Untersuchung dieser Komponenten liefert tiefere Einblicke in die Prozesse und Mechanismen, die einer gesunden Schwangerschaft unterliegen. Weitere vergleichende Arbeiten sind nötig, um ein Verständnis für diesen Aspekt der Schwangerschaft zu schaffen, weshalb die vorliegende Arbeit sich auf die fötal-maternale Verbindungschicht bei Meerschweinchen (*Cavia porcellus*) konzentriert. Wir analysieren die Zellzusammensetzung dieser Verbindung zu drei Zeitpunkten während der langen Schwangerschaft (6.5, 30.5, und 55 Tage nach Kopulation), sowie während des Diestrus im nichtbefruchteten Uterus. Dafür verwenden wir histologische Färbemethoden und erstellen eine grobe Beschreibung der Morphologie und der Zelltypen des reproduktiven Gewebes von Meerschweinchen. Zusätzlich vergleichen wir unsere Ergebnisse mit aktuellen Daten von single-cell RNA-Sequenzierungen generiert von Basanta & Stadtmauer (in prep.). Die größte Veränderung der fötal-maternalen Verbindung konnten wir zwischen dem Zeitpunkt der Implantation (6.5 dpc) und der mittleren Schwangerschaftsphase (30.5 dpc) feststellen. In diesem Zeitraum finden wichtige Prozesse wie die Dezidualisierung des Endometriums und die Bildung der plazentalen Strukturen statt, welche die utero-plazentale Verbindung der Meerschweinchen bilden. Diese beinhalten die akzessorische Subplazenta, die im Aufbau den Villi der chorio-allantoischen Plazenta des Menschen ähnelt. In der zweiten Hälfte der Schwangerschaft, nach dem luteo-plazentalen Shift in der Produktion von Progesteron, setzen Degenerationsprozesse ein. Diese umfassen die letztendliche Degeneration der Subplazenta und die Akkumulation von amorphen abgestorbenen Zellmassen innerhalb der breiten Verbindungszone, sogenannt „junctional zone“. Diese Zone trennt plazentales Gewebe von maternalem Dezidua und weist ein chaotisches Erscheinungsbild auf, das charakteristisch für diese Spezies ist. Diese Erkenntnisse verdeutlichen die Komplexität der fötal-maternalen Verbindung und ihrer Transformation im Verlauf einer Meerschweinchen-Schwangerschaft.

3. Introduction

Eutherian pregnancy is characterized by the close association between the mother and the developing embryo, namely the fetal-maternal interface (FMI). This interface is the locus of utero-placental exchange of gases and nutrients, as well as the locus of communication by hormones and other signaling molecules, which affect the maternal physiology and fetal development. Despite the placenta being a defining feature of placental mammals, and a feature determining reproductive success, it is also one of the most variable features of placental mammals, judging from what is known of the general placental comparative anatomy.

Due to their specific placentation process and extended pregnancy, an aspect particularly relevant when compared to other rodents, and even primates, guinea pigs are an important study organism for placental development and function. Knowledge about guinea pig gestation provides insights on human adult diseases that have long-term consequences for the offspring, both in humans and rodents (Aguilera, et al., 2022). The main characteristics of the early eutherian development are shared across species, yet details vary widely, in particular those concerning placentation.

During the initial stages of development after fertilization, the blastocyst undergoes differentiation, with the inner cell mass giving rise to the embryonic tissues, including the amnion, major components of the yolk sac and allantois. Simultaneously, the outer cell layer, the trophoblast, contributes to the formation of extra-embryonic membranes. That includes the endoderm of the yolk sac and the mesoderm, which interposes between trophoblast and endoderm. Later the allantois expands until in contact with trophoblast, synchronously fusing with chorionic mesoderm to form a chorio-allantoic placenta vascularized by allantoic vessels. In some species, including humans, only the chorio-allantoic placenta develops, whereas in others like lemurs and lorises, the yolk sac persists to support the developing embryo during early development, or until term, like in rodents and lagomorphs (Carter & Enders, 2004).

In the face of enormous variation in placentation across mammalian species, Grosser (1927) realized that this process can be classified with respect to the number of layers separating maternal and fetal blood. These are named by the apposed maternal and fetal tissues as hemo-, endothelio-, and epitheliochorial, with the former being the most invasive, and the latter being the least invasive. It has been inferred by Wildman et al. (2006) that the ancestral placentation of Eutherian mammals is of the hemochorial type. Less invasive placentation has repeatedly evolved in several lineages, generating a wide variation in invasiveness across species. Placentation in the two oldest Eutherian superorders Afrotheria and Xenarthra are either of endotheliochorial or hemochorial type. In the superorder Laurasiatheria every placentation type can be found. Several

species within Laurasiotheria have epitheliochorial placentas, Carnivores have the endotheliochorial type and bats and insectivores have endotheliochorial and hemochorial placentation. The fourth superorder of Eutherians are the Euarchontoglires, combining the sister groups Glires and Euarchonta, where all three types of placentation appear. The Glires, comprising Lagomorphs and Rodents, and the Dermoptera (Flying Lemurs) and higher Primates appertaining to Euarchonta, share the hemochorial placentation (Carter & Enders, 2004).

Hemochorial placentation was further subdivided by Enders (1965) with respect to the number of layers of trophoblast between the maternal blood space and the fetal blood vessels. This number ranges from hemomonochorial placentas, as found in humans and guinea pig, with one layer of syncytiotrophoblast, to hemotrichorial placentas with three different trophoblastic layers, as in mouse and rat. Advances in technology and scientific methodology have not only facilitated our understanding of placentation but have also expanded our understanding beyond the morphology of the interhemal space. Complementing the earlier classifications, Carter & Enders (2004) summarized the placentation processes of eutherians with focus on the trophoblast-variation.

Eutherians also share an innovation on the maternal side of the interface, namely decidual stromal fibroblast cell type, which is likely a cell type associated with enabling the evolution of implantation (Arendt, et al., 2016). Species with invasive trophoblast and hemochorial placentation share the formation of a decidual layer. This endometrial layer forms by differentiation of the maternal uterine stromal fibroblasts and coincides in most species with extended growth of endometrial glands. The forming decidual cells are of irregular polygonal shape with little cytoplasm, enlarged nuclei and increased cell size (Wooding & Burton, 2008).

In humans, the process of decidualization occurs in every ovarian cycle, regardless of the presence of a conceptus. It leads to a decidual zone, which is subsequently shed if the fertilization and concluding blastocyst implantation does not occur. This phenomenon is called “spontaneous decidualization” and is only observed in Old World monkeys, apes, the elephant shrew and one bat species. In certain groups of placental mammals, the decidualization reaction is not spontaneous but instead occurs in response to the implantation of a blastocyst, as e.g. in rodents (Emera, Romero, & Wagner, 2011). In early human pregnancy, maternal immune cells (uterine Natural Killer cells, macrophages, T lymphocytes, dendritic cells and B lymphocytes) make up about half of all cells within the decidual layer and the decidualization process is at its maximum (Wooding & Burton, 2008).

By the time the chorio-allantoic placenta is developing in humans, the proportion of invasive trophoblast cells in the fetal-maternal interface increases. The decidua supports placental growth

by producing nutrients and hormones and potentially acts as an immunological barrier or mediator between fetus and mother, e.g., as in mouse (Soncin, Natale, & Parast, 2015). During early to mid-pregnancy in humans, as the placenta and conceptus grows, the decidual zone stretches and decreases in width due to programmed cell death. At term, only a thin layer of decidual cells remains (Wooding & Burton, 2008).

Given this wide variation, the generalizations about reproductive traits across eutherians is difficult, and the choice of animal models specifically to model human reproductive traits or disease states must be done with caution. Myomorph rodents, in particular house mouse (*Mus musculus*), but also rat and hamster, are frequently used as model organisms in the fields of human reproductive anatomy and physiology. Especially mouse research substantially informed human reproductive biology, owing to the morphological similarities between the two species, such as the decidualization process or formation of a discoid chorio-allantoic placenta. However, there are also differences. For example, the mouse blastocyst implants into a narrow endometrial cleft instead of actively invading the endometrium (Croy, Yamada, DeMayo, & Adamson, 2014). Additionally, the interhaemal barrier consists of three layers: two layers of syncytiotrophoblast and one layer of cytotrophoblast. This *hemotrichorial* placenta consists of labyrinth, junctional zone and yolk sac and the maternal side comprises the metrial gland and decidua. Mice have a gestation length of 19 to 22 days and give birth to, on average, 6 to 8 altricial pups. Many of the mouse reproductive traits are rather derived and mouse is possibly not appropriate representative even of rodents.

Examining the outgroups of myomorphs, a more representative rodent for reproductive research was found, subjected to fewer studies than mice. The hystricomorph guinea pig has been proposed as a model that in many aspects of pregnancy appears more similar to human: prolonged pregnancy (60-70 days) and precocial neonates (Andersen, et al., 2018), progesterone production that shifts during pregnancy from the corpus luteum to the placenta, number of trophoblast layers (Aguilera, et al., 2022) and interstitial implantation (Wooding & Burton, 2008).

Duval (1892) was the first to write a detailed report on guinea pig placentation, nowadays regarded as the standard work. His pioneering work revelated an inversion undergoing yolk sac and the origin of placental syncytium from fetal ectoderm. As in human pregnancy, the guinea pig placentation is hemomonochorial and the chorio-allantoic placenta has a discoid shape. The fetal-maternal interdigitation in guinea pigs shares a labyrinthine pattern with mice, as opposed to the branching villi structure in human. The labyrinth forms in syncytiotrophoblastic lobes, surrounded by maternal blood.

Nevertheless, even given the similarities of guinea pig to the physiology of human pregnancy and placental function, there are fundamental differences in the anatomy and physiology between the species; including uterine shape, number of embryos, placental morphology, endocrine function, and metabolic requirements (Aguilera, et al., 2022).

Unique to hystricomorph rodents is an accessory villous “subplacenta” (as seen in Fig.1), which is located on the maternal side of the labyrinthine main placenta. Duval (1892) stated its origin from the chorionic ectoderm and Davies, Dempsey, & Amoroso (1961) verified this. The subplacenta connects the main placenta with the fetal-maternal junctional zone in guinea pig and serves as a source of extra-placental trophoblast cells that invade the FMI as far as the maternal decidua. The proliferating activity of the subplacenta is comparable to the placental cell columns active in trophoblast formation in humans. An exact function remains to be identified.

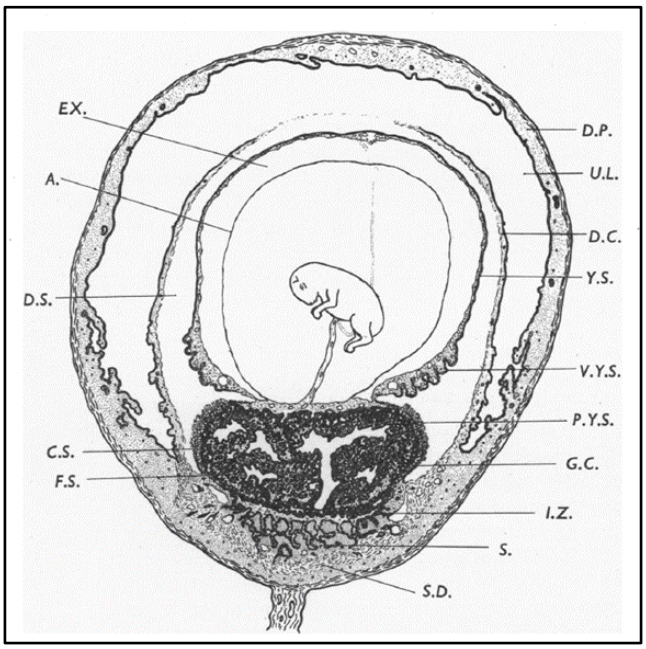

Figure 1 *“Diagrammatic cross-section of the guinea-pig uterus about the middle of pregnancy (35 days). A. amnion; C.S. coarse syncytium; D.C. decidua capsularis; D.P. decidua parietalis; D.S. decidual cavity; EX. exocoelom; F.S. fine syncytium; G.C. chorionic giant cells; I.Z. intermediate zone; P.Y.S. parietal wall of yolk sac; S. subplacenta (cytotrophoblast in solid black, syncytium stippled); S.D. subplacental decidua; U.L. uterine lumen; V.Y.S. villous part of visceral yolk sac; Y.S. visceral wall of yolk sac.” (Davies, Dempsey, & Amoroso, 1961)*

The junctional zone is a broadly used term in different species for differently located zones. In humans, the junctional zone is defined as subendometrial myometrium and connects the myometrium with the endometrium (Brosens, de Souza, & Barker, 1995). In mice, it is the avascular part of the chorio-allantoic placenta which builds the junction to the maternal site. It originates from cell differentiation from the ectoplacental cone and the secondary trophoblast giant cells, building one layer of trophoblastic giant cells and one layer of spongiotrophoblast and

glycogen trophoblast cells (Croy, Yamada, DeMayo, & Adamson, 2014). In guinea pigs, the term “junctional zone” is used by Wooding & Burton (2008) as a synonym for “spongiotrophoblast” and “trophospongium” located between subplacenta and main placenta. The junctional zone is also referred to as “subplacental decidua” (as depicted in Figure 1) by Davies, Dempsey, & Amoroso (1961), and forms the area between decidua basalis and a necrotic decidual layer. This latter definition will be used in following references to the junctional zone in guinea pig.

The fetal-maternal interface has been studied much less than the placental anatomy, in particular in non-model species, or in comparative fashion. A better understanding of the utero-placental interface and its evolution requires comparative information from multiple species, covering the important nodes of the phylogenetic tree of mammals. To contribute to this field, we here focus on the general anatomy and cell composition at the utero-placental interface of guinea pigs, using histology and single-cell transcriptomic data.

By close description of guinea pig fetal-maternal interface at the cellular level, we aim to contribute to the understanding of function and evolution of the eutherian fetal-maternal interface. We assume that the cell types of the guinea pig interface are sufficiently similar to the better understood mammalian models so that we will be able to recognize, and subsequently localize them. We will use the mouse counterpart as guidance.

This work addresses the following questions:

1. How does the guinea pig uterus during implantation stage differ from the non-pregnant control at diestrus?
2. Which cells are present in the utero-placental interface at mid and late gestation in guinea pig?

We expect that exploring the cell types of the guinea pig utero-placental interface will unveil new insights into mammalian pregnancy and its evolution. Their short gestation and lifespan (compared to human), enable us to obtain tissue samples from the maternal and fetal parts at any stages, which is also helpful for understanding the developmental processes.

4. Methods

4.1. Samples

The formalin-fixed paraffin-embedded samples of guinea pig reproductive tissues were previously obtained at three relevant time points during the reproductive cycle and gestation, corresponding to single cell data. The samples include uterine horns from non-pregnant diestrus (6.5 days after estrus), implantation stage at 6.5 days post copulation (dpc) and mid gestation at 30.5 dpc, each from one individual. In addition, embedded tissue samples were available from late gestation at 55 dpc. In order to accurately determine the pregnancy dating, each experimental group consisted of one male and one female guinea pig housed together in a cage for a duration of one day (dpc = 0), ensuring potential mating opportunities and subsequent gestational timing. The guinea pigs used for the late gestation tissue harvest were bred at the Cincinnati Children's Hospital Research Center and the tissue dissected in 2017. All other animals were bred in accordance with the animal welfare and ethics regulations of the University of Vienna. Tissue harvesting occurred at the university in 2022.

The duplex uterus of guinea pigs is formed as two separate uterine horns caudally forming the uterine body (Al-Saffar & Al-Ebbadi, 2019). The uterine horns of diestrus and implantation stage were divided and bisected, resulting in four segments, each of which was subsequently individually fixed in 4% Paraformaldehyde solution. Samples collected at mid gestation were fixated upon removal of the majority of the mesometrial uterine wall, the fetus and the labyrinth portion of the chorio-allantoic placenta. Consequently, the remaining tissue includes the myometrium (anti-mesometrial uterine wall), the fetal-maternal interface and the subplacenta. The same procedure was applied to the tissue of the late gestation stage at 55 dpc, except the full chorio-allantoic placenta was maintained. For further processing, all dissected tissue sections were first dehydrated and then embedded at 60°C in paraffin.

Microtomes (specifically Leica SuperCut and Leica RM2265) were used for generating longitudinal paraffin sections with a thickness of 5µm. Following a 50°C water bath, the sections were affixed onto Superfrost® Plus microscope slides and allowed to air-dry. The slides with sections in close proximity to the center of the utero-placental interface were selected for the staining procedures.

4.2. Staining for molecules

For qualitative assessment of the morphology and architecture of tissue we used hematoxylin and eosin (H&E) staining, following the standard protocols, with 40 seconds in Mayer's hematoxylin

and 1 minute in eosin. The staining highlights the acidic components, such as nuclei, in blue-purple, while basic components like cytoplasm and extracellular matrix appear pinkish.

To visualize collagen fibers, muscles and mucin, we used the Masson's Trichrome Staining, according to the protocol from IHC World, LLC. (2023). Collagen and mucin stained blue, while muscle fibers stained red. Minor adjustments were made to the protocol, specifically reducing the duration of incubation in Weigert's iron hematoxylin and the subsequent rinsing in tap water to 5 minutes, as opposed to the standard 10 minutes.

To assess carbohydrates, and specifically quantify glycogen, we used Periodic Acid-Schiff (PAS) and PAS-diastase (PAS-D) staining with a modified step. For a qualitative comparison, the staining was conducted on neighboring and semi-neighboring slides. The PAS staining protocol was from IHC World, LLC. (2023). The PAS-D staining followed the same procedure, with an additional incubation in 1 mg/ml of α-amylase for 30 min at 37°C after the initial deparaffinization and hydration. In PAS staining, instead of the amylase treatment, the slides were incubated in distilled water (Chavan & Wagner, 2016). PAS stain colors carbohydrates pink, whereas the same portions appear without color by degradation of glycogen through amylase.

The mounting medium used for cover slipping in all stainings was Permount™ (Thermo Fisher Scientific Inc., D-Schwerte).

4.3. Staining for proteins

We used fluorescent immunohistochemistry (IHC) to localize cell clusters in the tissue by their expression of specific marker proteins. Several experiments were performed on the paraffin slides, using primary antibodies (AB) specific to particular proteins (listed in Table 1), followed by a secondary antibody against the primary AB and conjugated with a fluorochrome.

We used a standard protocol, adapted within the laboratory. The first step involved heating the slides at 60°C overnight in the oven. The following morning, deparaffinization was carried out through three changes of xylene (10 min each), followed by rehydration through three changes of 100% Ethanol (EtOH) and 95% EtOH (20 dips, 3 min, 20 dips, each), two changes of 70% EtOH (20 dips, 3 min, 20 dips, each) and a 5 min wash in PBS.

For antigen retrieval, the slides were then placed into Coplin jars, covered by citrate buffer (pH 6.0, 10x). The jars were placed into a plastic container filled with deionized (DI) water. The plastic container with jars was put into a microwave oven, and microwaved at 800W for 6:30 min, followed by 300W for 12 min. While still in the citrate buffer, the slides were cooled in a bucket of cold water and ice for 15 min, then rinsed in DI water and cleared in PBS.

The removal of endogenous peroxidase activity was mediated by incubation in a mixture of methyl alcohol and hydrogen peroxide (30%) at room temperature (~21°C). The slides were then washed in PBS for 5 min. To prevent non-specific binding, the tissues were incubated in blocking serum (BSA amount = 5% of TBS-Tween amount) for one hour at room temperature.

The tissue slides were incubated in a primary AB/ blocking serum mixture at room temperature in a darkened humidified slide box for one hour. The primary AB dilution was optimized with references from the ©1998-2023 Abcam plc. (n.d.) website. After washing the slides in TBS-Tween (0,1%) solution five times (20 dips, 3 min, 20 dips, each). The same procedure was repeated with the secondary antibody. Finally, the slides were coverslipped with ProLong™ Diamond Antifade Mountant with DAPI (Invitrogen by Thermo Fisher Scientific, D-Schwerte).

The selection of primary antibodies was based on the proteins of interest and the compatibility with mouse reproductive tissue, as hardly any antibodies specific for guinea pig are available. This study hence tested mouse antibodies on guinea pig to elucidate the general structure and cells of the fetal-maternal interface. All antibodies utilized in this master's thesis were purchased by the Pavličev laboratory from ©1998-2023 Abcam plc. and are explicitly listed in Table 1.

Primary Antibody	Abcam nr.	Host	Dilution	Marker for
Anti-CD11b	ab133357	rabbit (monoclonal)	1:500	monocytes & neutrophils, cell surface
Anti-CD45	ab10558	rabbit (polyclonal)	1:100	immune cells, transmembrane
Anti-Cytokeratin 7 (CK7)	ab181598	rabbit (monoclonal)	1:200	cytoskeleton of glandular & luminal epithelium, & trophoblast
Anti-Cytokeratin 19 (CK19)	ab52625	rabbit (monoclonal)	1:1000	similar to CK7
Anti-Ki67	ab16667	rabbit (monoclonal)	1:200	proliferating cells
Anti-Oxytocin-neurophysin 1	ab212193	rabbit (monoclonal)	1:500 & 1:8000	Oxytocin-expressing cells
Anti-SDF1	ab25117	rabbit (polyclonal)	1:100	cell migration
Anti-Vimentin	ab11256	goat (polyclonal)	1:100	cells of mesenchymal origin, intermediate filaments
Anti-Vimentin (VIM)	ab92547	rabbit (monoclonal)	1:200	mesenchymal cells, cytoskeleton

Table 1

Primary antibodies retrieved from rabbits were paired with the secondary antibody Goat Anti-Rabbit (Alexa Fluor® 488; ab150077, dilution 1:1000).

The primary antibody Anti-Vimentin retrieved from goat was paired with the secondary antibody Donkey Anti-Goat (Alexa Fluor® 647; ab150131, dilution 1:250).

4.4. Staining for mRNA

The 2.5 HD Assay-BROWN kit (Cat No: 322300, Advanced Cell Diagnostics) with Pecam-1 target probe was utilized for the RNAscope™ experiment. This kit employs brown chromogens and hematoxylin (Gill's), resulting in the staining of targeted RNA molecules in brown and cell-nuclei in blue. Pecam-1 is a cell surface protein expressed in platelets, vascular endothelial cells and leukocytes. The protocol for the RNAscope™ experiment derived from the kit's user manual.

4.5. Analysis

Negative controls for each staining and an additional positive control for the RNAscope™ run were included but not shown in this master's thesis. However, the controls provided support for the interpretations presented.

The microscope EVOS™ M700 (Invitrogen by Thermo Fisher Scientific, D-Schwerte) was used for imaging the stained tissue slides. The images were captured at different magnifications (10x, 20x and 40x) for overall view or to highlight specific cell regions of interest.

Tissues on slides treated with non-fluorescent staining methods (as described in 3.2. Staining for molecules, and 3.4. Staining for mRNA) are visible in transmitted white light under the microscope.

In contrast, tissue slides subjected to IHC were predominantly imaged in the GFP (green fluorescence protein) light channel (wavelength: 530nm) and RFP (red fluorescence protein) light channel (wavelength: 600nm). Thus, the cells expressing the target protein appear green, while the background autofluorescence reflects in broad range. Tissue exceeding 5 µm, due to erroneous section cutting, and erythrocytes will thus appear yellow to red due to the dual reflection and can be recognized. Some images were taken with the DAPI light channel (wavelength: 450nm) in search for cell nuclei in specific areas of the FMI. They feature a blue background, with other attributes as described before. Yet other images were captured solely in GFP channel, displaying various intensities of green.

Finally, scale bars were inserted in all images with EVOS™ Analysis software and the images were adjusted for brightness and contrast using Windows Photo Viewer.

4.6. Abbreviations

AB, antibody; *CGC*, chorionic giant cells; *CK7*, anti-cytokeratin7; *CK19*, anti-cytokeratin19; *CY*, cytotrophoblast; *DB*, decidua basalis; *DC*, decidua capsularis; *DGC*, decidual giant cells; *DI*, deionized; *dpc*, days post copulation; *DP*, decidua parietalis; *DS*, deep stroma; *E,* endometrium; *ECM*, extracellular matrix; *EG,* endometrial glands; *EtOH*, ethanol; *EXM,* external myometrium; *EPTC*, extra-placental trophoblast; *FMI*, fetal-maternal interface; *FV*, fetal vessel; *H&E*, hematoxylin and eosin (staining); *IHC*, immunohistochemistry; *IM,* internal myometrium; *IZ*, intermediate zone; *JZ*, junctional zone; *M,* myometrium; *MA*, maternal artery; *MB*, maternal blood space; *PAS*, Periodic Acid Schiff; *PE*, parietal endoderm; *S*, syncytium; *scRNA-seq*, single-cell RNA-sequencing; *SF*, superficial stroma; *SP*, subplacenta; *SYN*, syncytial streamer; *TGC*, trophoblastic giant cells; UC, umbilical cord; *UL,* uterine lumen; *VIM*, anti-vimentin (rabbit monoclonal antibody); *VL,* vascular layer; *VYS*, visceral yolk sac

5. Results

5.1. The non-pregnant uterus (Diestrus)

The uterine horn of the non-pregnant guinea pig consists of myometrium (M), endometrium (E) and uterine lumen (UL), which can be distinguished by microscopic examination of the H&E-stained tissue samples, as shown in Figure 2.

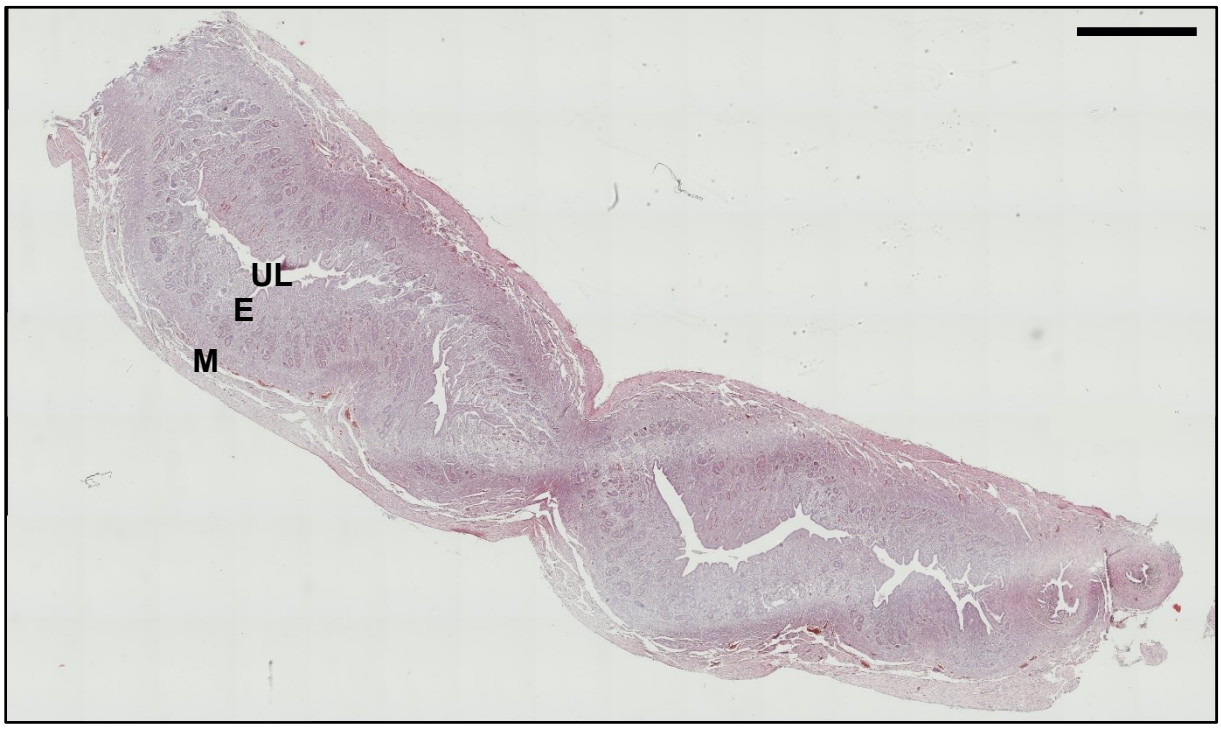

Figure 2 *longitudinal section of the uterine horn of* ***non-pregnant*** *guinea pig, dissected 6 days after Estrus (in Diestrus), overview for the later in detailed described areas; the endometrium (E) lines the uterine lumen (UL) and is encircled by the myometrial layers (M), the thin perimetrium is not recognizable in this image. H&E. Scale bar: 1000 µm.*

The outermost layer of the uterus, known as the perimetrium, encircles the organ as a thin sheath. It remains indistinguishable from the myometrium under H&E staining (see Fig.2). Identified as serosa, the perimetrium consists of a mesothelial layer on the outer surface and an underlying vascularized connective tissue layer. They become discernable through Masson's Trichome staining (as in Fig.3a), revealing a blue-stained connective layer with red stained fragments of mesothelium.

The perimetrium rests on longitudinal bundles of smooth muscle fibers forming the outer myometrium. The inner myometrium consists of circularly oriented smooth muscle fiber bundles. In Masson’s Trichrome staining, smooth muscle cells are stained red, whereas interspacing collagen of the extracellular matrix is blue-stained. The two myometrial muscle layers are

separated by a loose vascular layer, which is constructed of blood vessels within a loose network of connective tissue. The latter appears in blue color due to the substantial collagen synthetization of the fibroblasts.

Arteries are surrounded by thin endothelium, resting on a basement membrane, a layer of collagen fibers and a wall comprising smooth muscle cells and fibroblasts. In Masson's Trichrome staining, the wall elements present as red cells with a blue interlayer (see Fig.3b). The vessels are surrounded by collagen fibers and fibroblasts. Capillaries throughout the uterine wall only have an endothelium with associated myofibroblasts (pericytes).

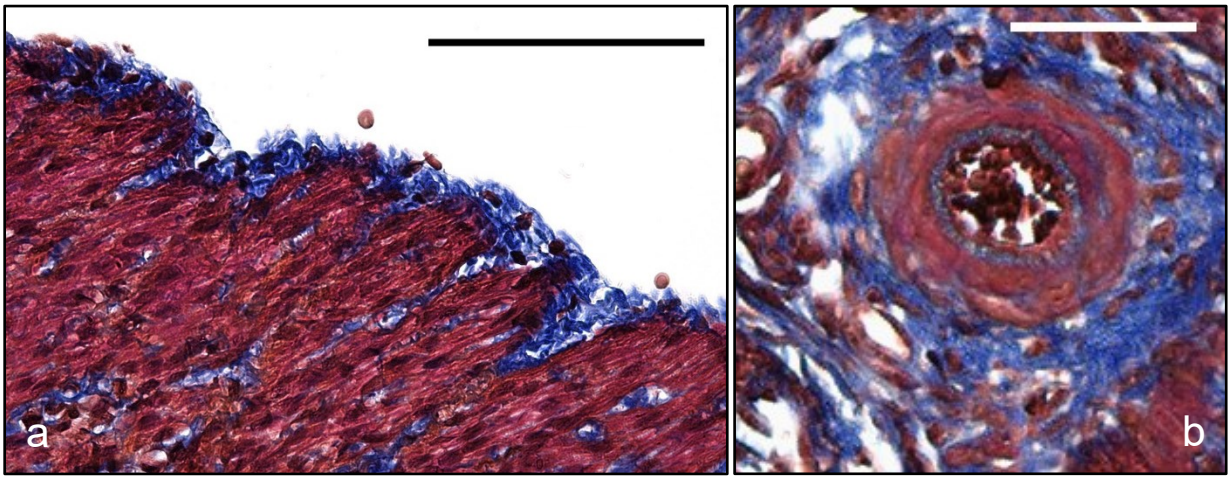

Figure 3 *sections of the* ***non-pregnant*** *uterus. Masson's Trichrome Staining.*
a) longitudinal bundles of smooth muscle fibers, stained in red (bottom), underlie vascularized blue-stained connective tissue of the perimetrium; the mesothelial layer of the perimetrium appears to be ruptured, but is still discernible in the upper left corner as red stained cells. Scale bar: 100 µm.
b) an artery within the vascular layer between internal and external myometrium, featuring red-stained endothelium, blue-stained collagen separating endothelium from artery wall; a composition of red-stained muscle cells and blue-stained collagen from fibroblasts form the arterial wall. Scale bar: 50 µm.

Within the endometrium of the non-pregnant guinea pig uterus, we observe a deep stroma (DS) characterized by a dense network of thick collagen fibrils (shown in Fig.4). Vascularization of the endometrium increases towards the uterine lumen, coinciding by a decrease of collagen density. The sub-luminal connective tissue is referred to as superficial stroma (SF).

The uterine lumen is lined by simple columnar epithelium, invaginated to different extents into the underlying superficial stroma. Endometrial glands (EG) feature the same columnar epithelium (Croy, Yamada, DeMayo, & Adamson, 2014) and are situated in the superficial and deep stroma throughout the endometrium. The enodmetrial glands are of differing but increasing size towards the myometrium.

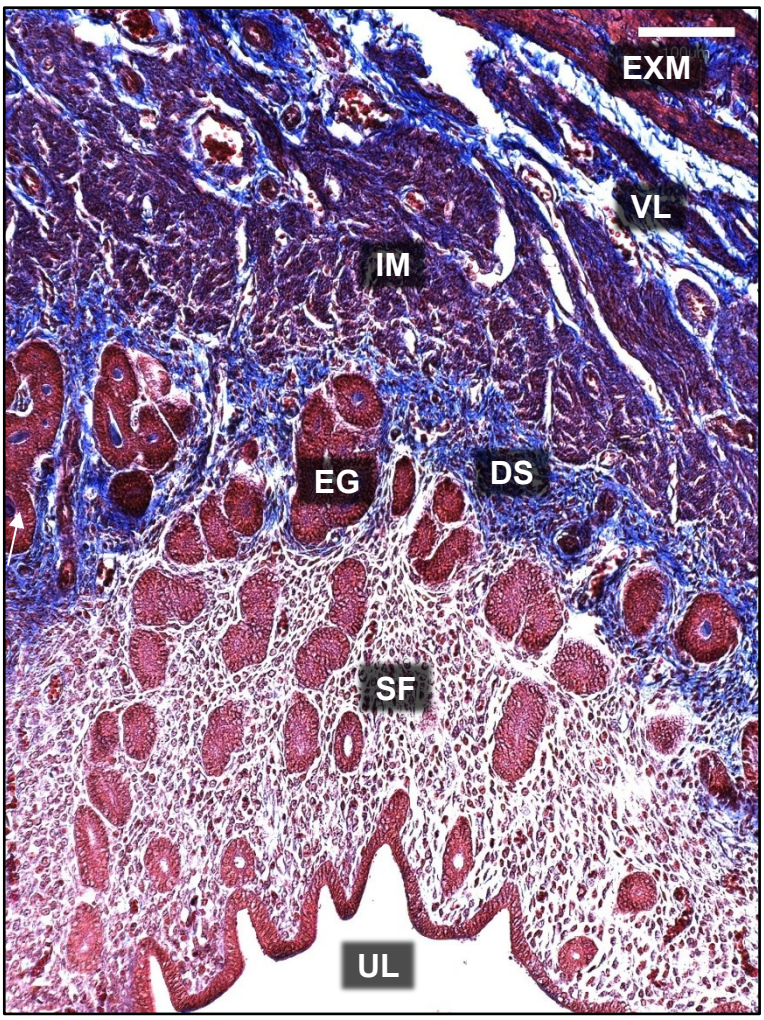

Figure 4 *longitudinal cross-section of the guinea pig* ***non-pregnant*** *uterine horn, dissected 6 days after Estrus; the myometrium divides into three layers: external myometrium (EXM), vascular layer (VL) and internal myometrial layer (IM); within endometrium, a layer rich in collagen (stained blue) is observed, the so-called deep stroma (DS), alongside a zone with low concentration of connective tissue, referred to as superficial stroma (SF), surrounding the uterine lumen (UL); the luminal epithelium, and the epithelium and secretion of endometrial tubular glands (EG) are stained red; the glands are distributed throughout the endometrium. Masson's Trichrome Staining. Scale bar: 100 µm.*

The epithelial cells including uterine luminal epithelium and gland epithelium show strong cytokeratin-immunoreactivity (see Fig.5a). The mesenchyme-derived outer wall of the uterus, the perimetrium, consists of vimentin-expressing cells (see Fig.5b). Smooth muscle cells of the myometrium do not express vimentin, but fibroblasts, pericytes and endothelial cells around blood vessels do exhibit VIM-signal. Stromal fibroblasts within the endometrium are abundant and show great immunoreactivity for anti-vimentin.

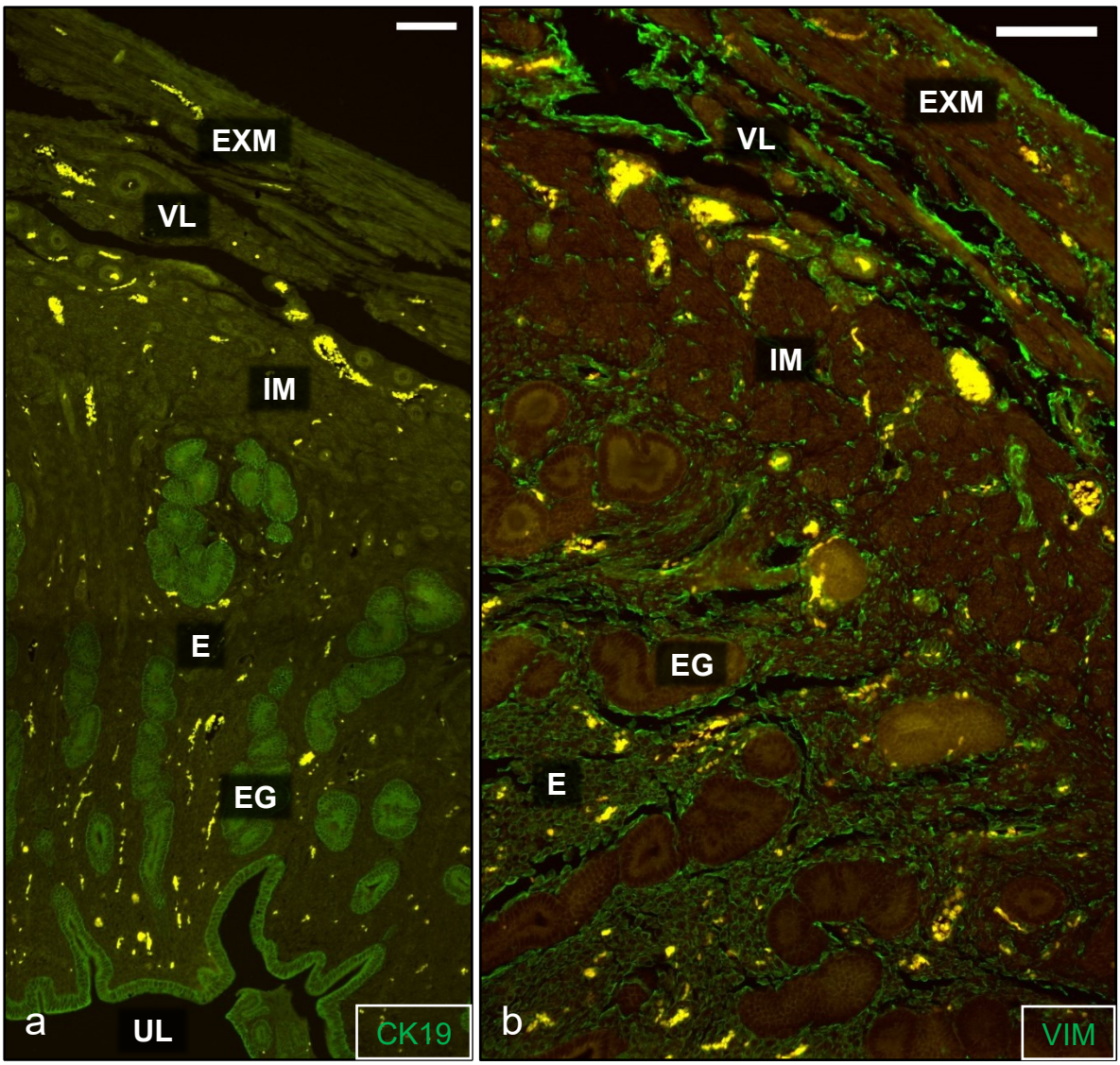

Figure 5 *immuno-stained* ***non-pregnant*** *uterine horn components include uterine lumen (UL), endometrium (E) with endometrial glands (EG), internal myometrium (IM), vascular layer (VL) & external myometrium (EXM). Scale bar: 100 µm. (signal: green; autofluorescence: yellow)*
a) *endometrial gland epithelium and luminal epithelium show cytokeratin-immunoreactivity. IHC for CK19.*
b) VIM-positivity is observed in fibroblasts, pericytes, mesenchymal cells and endothelial cells throughout the uterus, and in stromal fibroblast cells within the endometrium. IHC for VIM.

The brown staining of the Pecam1 mRNA (see Fig.6) reveals the presence of vascular endothelial cells. As illustrated in Figure 6a, Pecam1-positive cells predominantly occur on one side of the endometrial superficial stroma. However, all other stainings show an even distribution of erythrocytes on both sides of the uterine lumen. The unilateral staining of the superficial stroma suggests the likely accumulation of immune cells instead of endothelial cells in that region, as Pecam1 is also expressed in platelets and leukocytes. Noticeable are the brown dots in

endometrial glands, also indicating immune cells. In the deep stroma and myometrium, we observe a limited presence of both cell types (see Fig.6b).

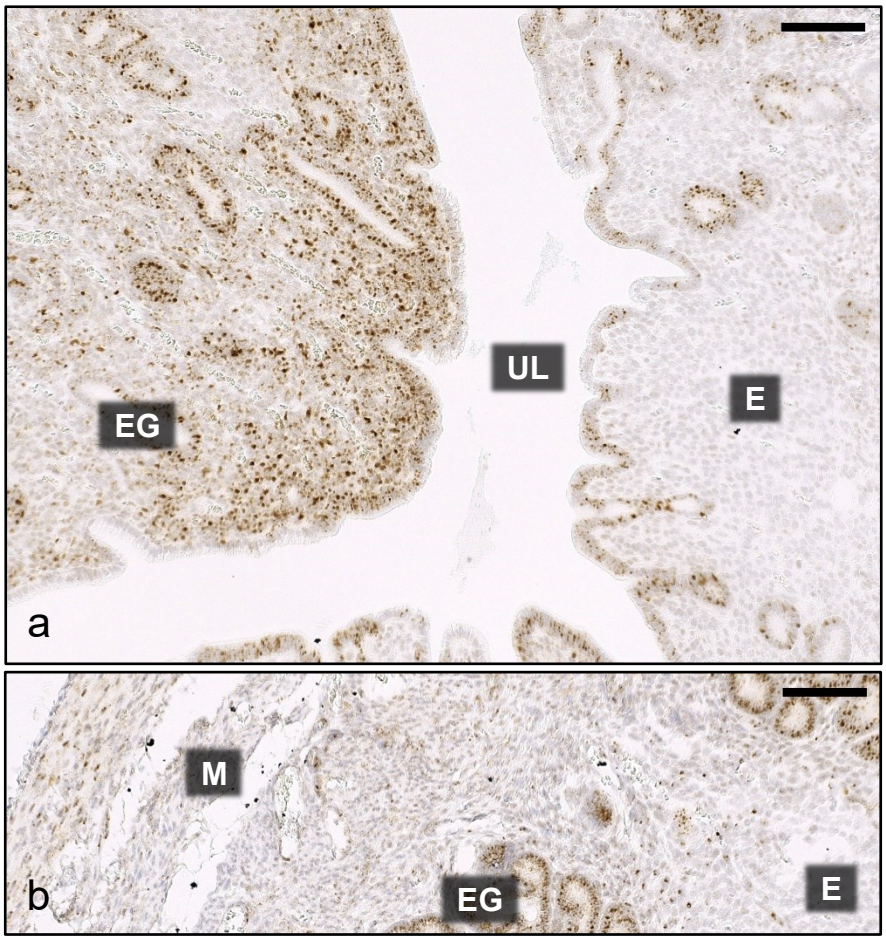

Figure 6 *section of the* ***non-pregnant*** *guinea pig uterine horn in diestrus, stained with Pecam1 using RNAscope™, Pecam1 expression is indicated by brown color. Scale bar: 100 µm.*
a) unilateral accumulations of Pecam1-expressing cells are observable adjacent to the uterine lumen (UL) in the endometrium (E); gland epithelium (EG) shows high expression, while luminal epithelium shows low expression of Pecam1 throughout the uterus.
b) the section shows myometrial layers (M) on the left to endometrium on the right; Pecam1 expression is predominantly observed in endometrial gland epithelium, but individual endothelial cells and immune cells are detected throughout the uterine tissue.

All our sections of non-pregnant uterine horns show a semi-continuous uterine lumen throughout the tissue. Exceptions are due to ruptured sections and peripheral tissue cuts. Tissue proliferation primarily occurs in the epithelial cells lining glands and lumen, within vascular walls and in the stroma of the endometrium, as indicated by Ki67 antibody staining. Single Ki67-expressing cells were also observed within the myometrial layers. However, they were not abundant.

5.2. The implantation uterus (6.5 dpc)

After successful fertilization, the developed blastocyst attaches to the anti-mesometrial side of the uterine lumen. In guinea pig, the attachment happens around day 6 and 7 post-copulation (Wilson, 1927; Canizo, Zhao, & Petropoulos, 2024). Our tissue samples were dissected on 6.5 dpc, therefore we first searched for a blastocyst to assure that an impregnation did happen. In this time period, we expect to find a blastocyst still disengaged in the uterine lumen or currently attaching.

We identified one potentially embryo-related cell cluster (see Fig.7a-b) in our samples. The found cluster is not yet attached to the luminal epithelium and is situated near the anti-mesometrial side within the uterine cavity, surrounded by mucous. The cells are compact, and no distinct blastocoel (cavity of the blastocyst) is observable, which suggests that the cells are still in morula stage. However, this stage normally ends on day 4 post copulation.

In H&E staining, we can recognize a relatively similar amount of acidic (react with basic purple hematoxylin) and basic (react with pink acidic eosin) cells. The zona pellucida is not indicated in Figure 7 but should still be present at this time point and not disappear until the attachment process started (Enders & Schlafke, 1969). In Figure 7a, basophilic fragments (purple) are situated at the bottom of the cluster, which may indicate processes of the abembryonic trophoblast of a blastocyst penetrating the zona pellucida. Enders & Schlafke (1969) researched the guinea pig blastocyst using Azure B staining, revealing that the zona pellucida has no affinity to this dye, which may be a similar case in our H&E staining. Another suggestion is that it may have dissolved in H&E staining during the eosin incubation because of low pH, and in IHC staining during the antigen retrieval step due to high temperature. Supporting this predication is the empty but round space between cell cluster and mucous.

In summary, the morphology indicates morula stage, although the time point aligns with the blastula stage, suggesting either an abnormality or a halted development of the morula. For the purpose of discussion, this cell cluster will be referred to as the “embryo-related cell-cluster”.

As the material was insufficient for all stainings, we do not have evidence for cytokeratin-immunoreactivity in the embryo-related cell cluster. Vimentin-positive cells are in the center of the cluster suggesting potential development of the inner cell mass in the blastocyst (see Fig.7c-d). The outer sheath of the embryo-related cell cluster is non-reactive to anti-vimentin, except for some particles (Fig.7c). It is important to note, that preimplantation development in mammals inherently involves a high degree of stochasticity in expression of these transcription factors. Their presence or absence does not definitively predict the future lineage fate.

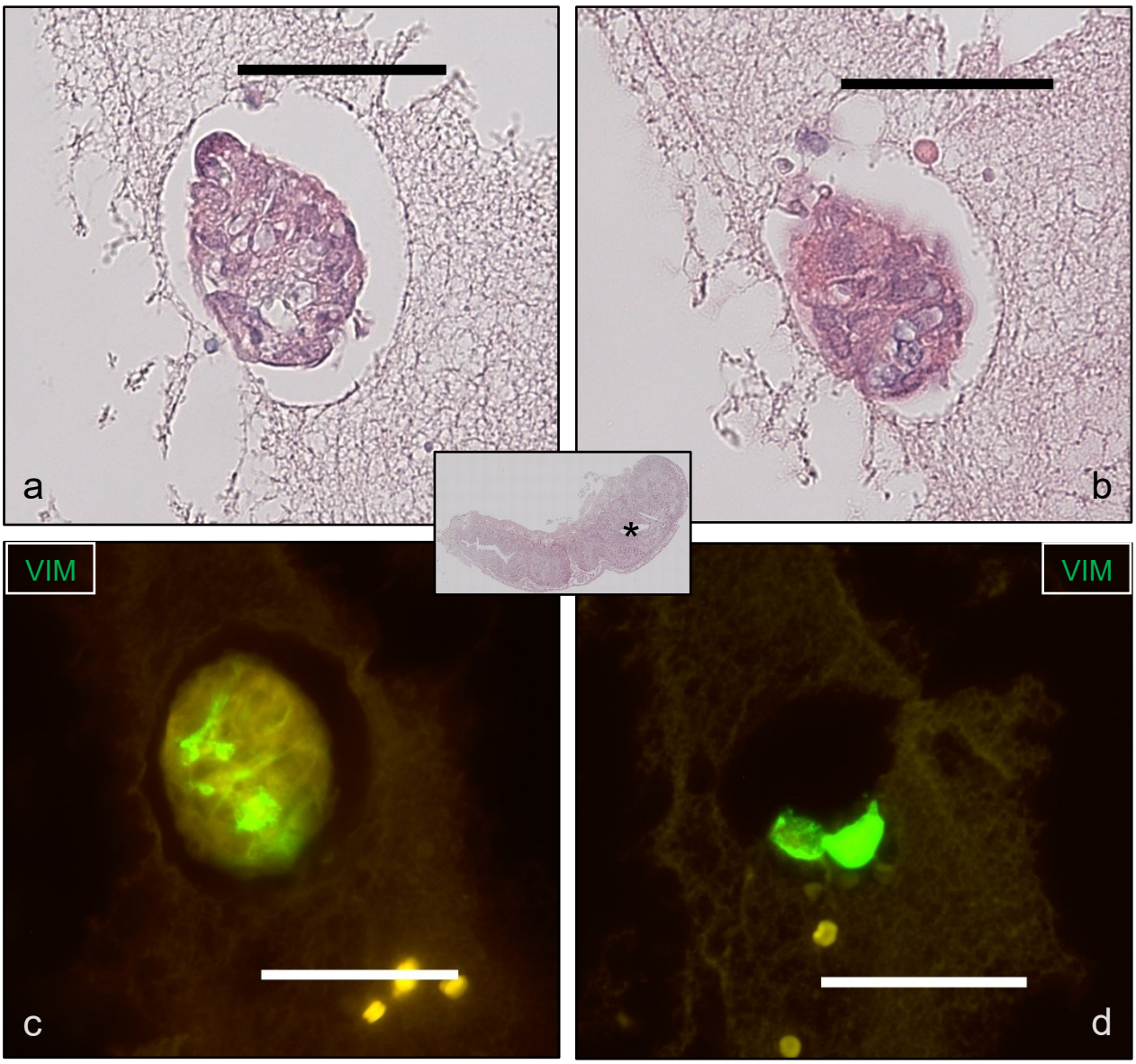

Figure 7 *cell cluster in guinea pig uterine lumen at* ***6.5 dpc****; neighboring sections; the inner image serves as an overview for the location of the section. Scale bar: 50 µm. (signal: green; autofluorescence: yellow) a)-b) the nearly round cluster shows different portions of acidic (purple) and basic (pink) components, apparent mitotic activity is observable in the cells, luminal mucosa surrounds the cell cluster. H&E. c) VIM-positive cells are situated within the cluster; the outer sheath displays varied reactivity against anti-vimentin, but the main part is auto-fluorescent, as are erythrocytes in the lower right corner. IHC for VIM. d) two intensely VIM-immunoreactive cells surrounded solely by mucosa and erythrocytes. IHC for VIM.*

Since our tissue samples were likely dissected at preimplantation, we can still observe the basic three-layered pattern of the uterus. Through Masson's Trichrome staining, shown in Fig. 8a, both myometrium and endometrium are clearly recognizable while the perimetrium is again only visible as blue and red fragments around the uterine horn. Indications of decidualization or development of fetal tissue are absent, aside from the presence of the embryo-related cell cluster.

The deep stroma of the endometrium appears with less densely packed collagen fibers in the extra-cellular matrix (ECM) on the mesometrial side (see Fig. 8b). This phenomenon is likely due to oedema formation in preparation for morphological alternations in the pregnant uterus. The deep stroma on the anti-mesometrial side is still constructed with a dense network of collagen fibers. The superficial stroma surrounding the uterine lumen has tightly associated endometrial cells with low collagen concentration. Remarkably, there are abundant, but small endometrial glands present in the superficial stroma, but many of even and great size in the deep stroma.

The implantation of guinea pig blastocyst is accompanied by stromal proliferation, hence progressive closing of the uterine lumen (Wilson, 1927), as evident in our tissue and observable in Figure 8a. In our other samples of uterine horns at 6.5 dpc, a similarly narrow and discontinuously open uterine lumen is observed across the examined depths.

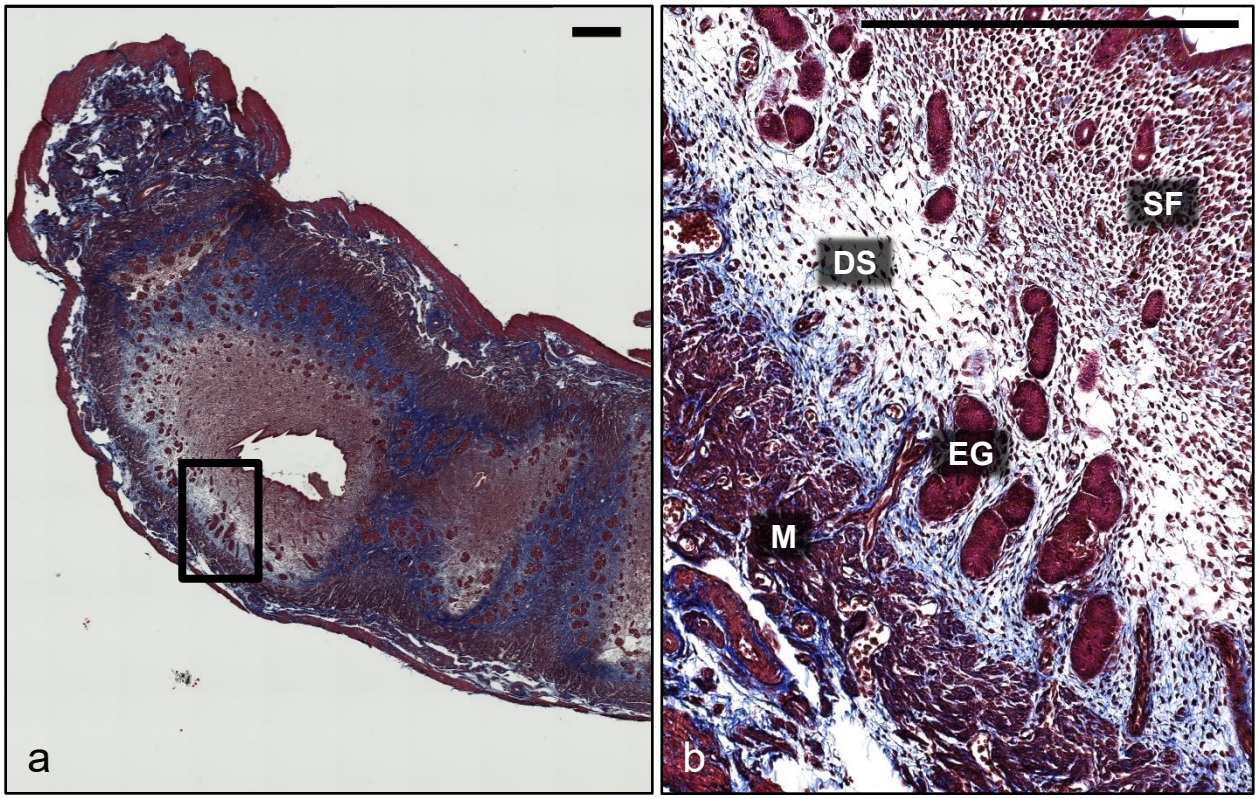

Figure 8 *longitudinal section of the guinea pig uterine horn at* ***6.5 dpc****; the rectangle in a) represents the location of the section in b). Masson's Trichrome staining. Scale bar: 500 µm.*
a) *the superficial stroma of endometrium is mainly stained red; the deep stroma has a dense blue-stained collagen network between fibroblasts on the anti-mesometrial side and a loose network on the mesometrial side; endometrial glands are numerous and of great size in the deep stroma, in contrast to the small glands of the superficial stroma; the uterine lumen is discontinuous.*
b) section of the myometrium (M) (lower left) to uterine lumen (upper right); the endometrium has large extracellular spaces in the deep stroma (DS) and a narrow cell network in the superficial stroma (SF); endometrial gland (EG) size increases towards myometrium.

Immunoreactivity of the proliferation marker Ki67 is detected in the stromal cells of endometrium, vascular walls across various layers, and epithelial cells lining the uterine lumen and glands. Individual Ki67-positive cells are identified in the myometrium. Cytokeratin- and vimentin-expressing cells are found in the same pattern as in the non-pregnant uterine horns. As can be seen in Figure 9, glandular and luminal epithelium show cytokeratin7-positivity, with numerous small, evenly sized endometrial glands present in the superficial stroma.

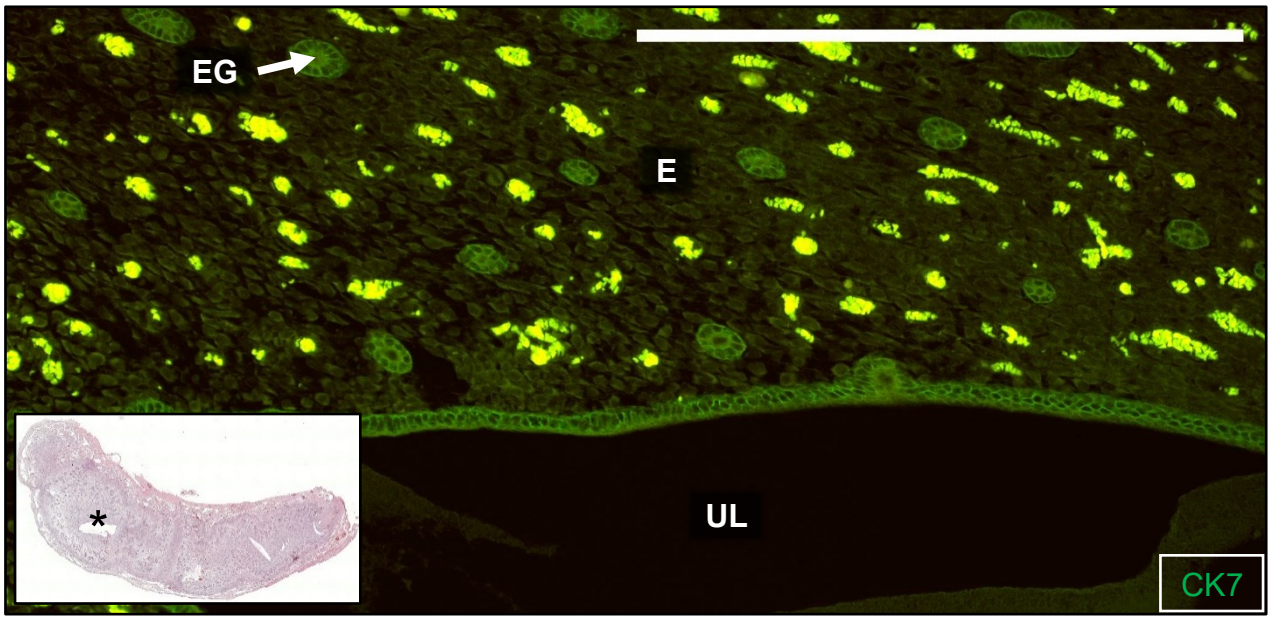

***Figure 9** uterine lumen (UL) and endometrium (E) with endometrial glands (EG) of the guinea pig uterine horn at **6.5 dpc;** the epithelium of lumen and glands is cytokeratin7-positive. IHC for CK7. Scale bar: 500 µm. (signal: green; autofluorescence: yellow)*

Pecam1 expression is sparsely detected in the superficial stroma of the endometrium, but evenly distributed in the deep stroma and myometrial layers. Nonetheless, its localisation at this stage is primarily in the epithelium of glands and lumen.

5.3. The fetal-maternal interface at mid gestation (30.5 dpc)

In guinea pig the time span of the implantation process comprises about 19 days starting on day six post copulation until day 25 of gestation (Davies, Dempsey, & Amoroso, 1961). An evident increase in fetal tissue and in the fetal-maternal interface is the result. Additionally, the uterus undergoes considerable changes during this period, altering the endometrium dramatically.

Stromal fibroblasts of the endometrium transform by steroid hormone-dependent division, enlargement, and differentiation into decidual secretory cells, changing its cell function irreversibly and supporting the implanting blastocyst (Kirkwood, et al., 2021). The cell morphology changes from uninucleate spindle-like shaped fibroblasts to uni- and multinucleate irregularly shaped

decidual cells with little cytoplasm and an enlarged perinuclear zone. By now, endometrial glands are entirely absent as decidual cells take over the hormone secretion (Wooding & Burton, 2008). Once decidual cells are established, we find the three subtypes of decidual layers. The decidua parietalis (DP) lines the uterine lumen outside the implantation site, transitioning into the decidua basalis (DB), which is in contact with the trophoblast (see Fig.10). The membrane enclosing the embryo and separating decidual from uterine cavity is the decidua capsularis (DC).

On day 30.5 after copulation the myometrial layers are more compact and stretched, and difficult to distinguish from the decidua basalis. Vascular layer (VL), internal (IM) and external myometrial layer (EXM) are not identifiable in our mid-gestational sections (as can be seen in Fig.10). In H&E staining the myometrium appears in a slightly lower intensity of pink than the decidua. DC and DP are partly implied on the right side of Figure 10. In the following, we will focus on the decidua basalis as it is an active part of the fetal-maternal interface.

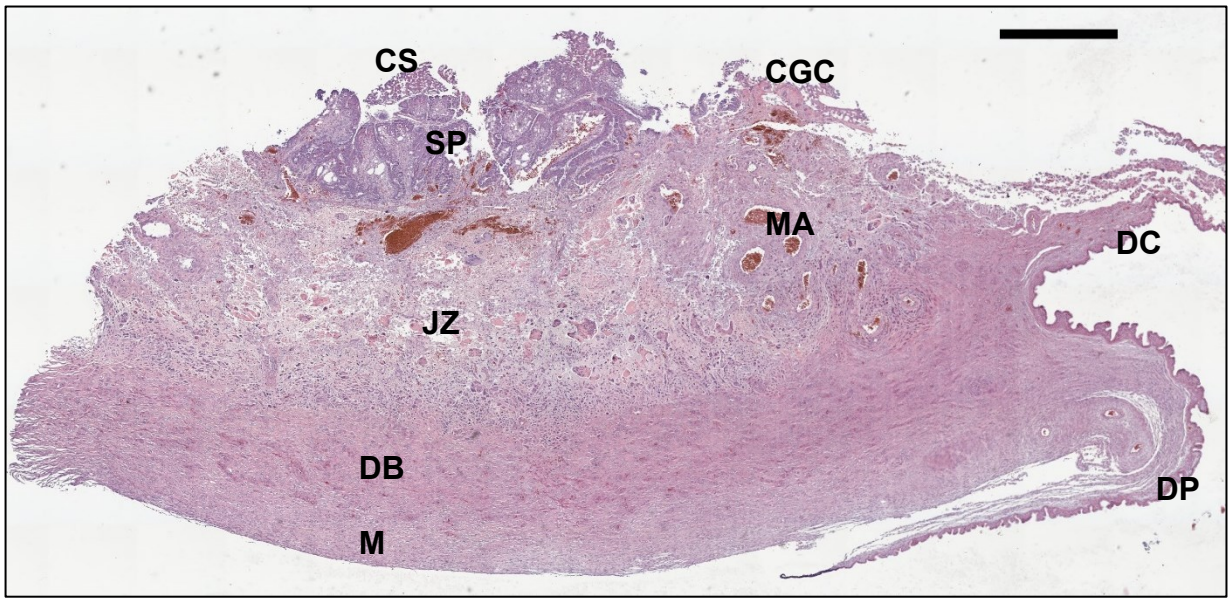

Figure 10 *longitudinal section of guinea pig uterus and fetal-maternal interface at* ***30.5 dpc****, overview for the later in detailed described areas; zones from bottom to top: myometrium (M), decidua basalis (DB), junctional zone (JZ) with subplacental decidua, necrotic decidua and maternal arteries (MA), subplacenta (SP) and parts of the coarse syncytium (CS) from the main placenta; chorionic giant cells (CGC) are on the margin of the subplacenta, and decidua capsularis (DC) and decidua parietalis (DP) are indicated on the right. H&E. Scale bar: 1000 µm.*

Carter et al. (1998) observed that guinea pig myometrium and decidual cells are not cytokeratin-immunoreactive, whereas our evaluation of the cytokeratin-experiments showed opposite results concerning the decidua. Both, cytokeratin7 and -19 are expressed in the decidual layer but not in myometrial muscle cells (see Fig.11a). The latter coincides with our results from the implantation phase and the non-pregnant uterus, where myometrium is also not immunoreactive against anti-

cytokeratin. The intensity of cytokeratin-expression within the decidual layer decreases towards the myometrium. The immunoreactivity against anti-vimentin was observed to vary in intensity in both the myometrium and decidua (see Fig.11b). This finding is unexpected, considering the lack of immunoreactivity observed in smooth muscle cells at earlier time points. Nonetheless, the cell network of the myometrium in our samples is dense and stretched, wherefore the vimentin-immunoreactivity can be attributed to the pericytes, fibroblasts and endothelial cells interspersed among smooth muscle cells.

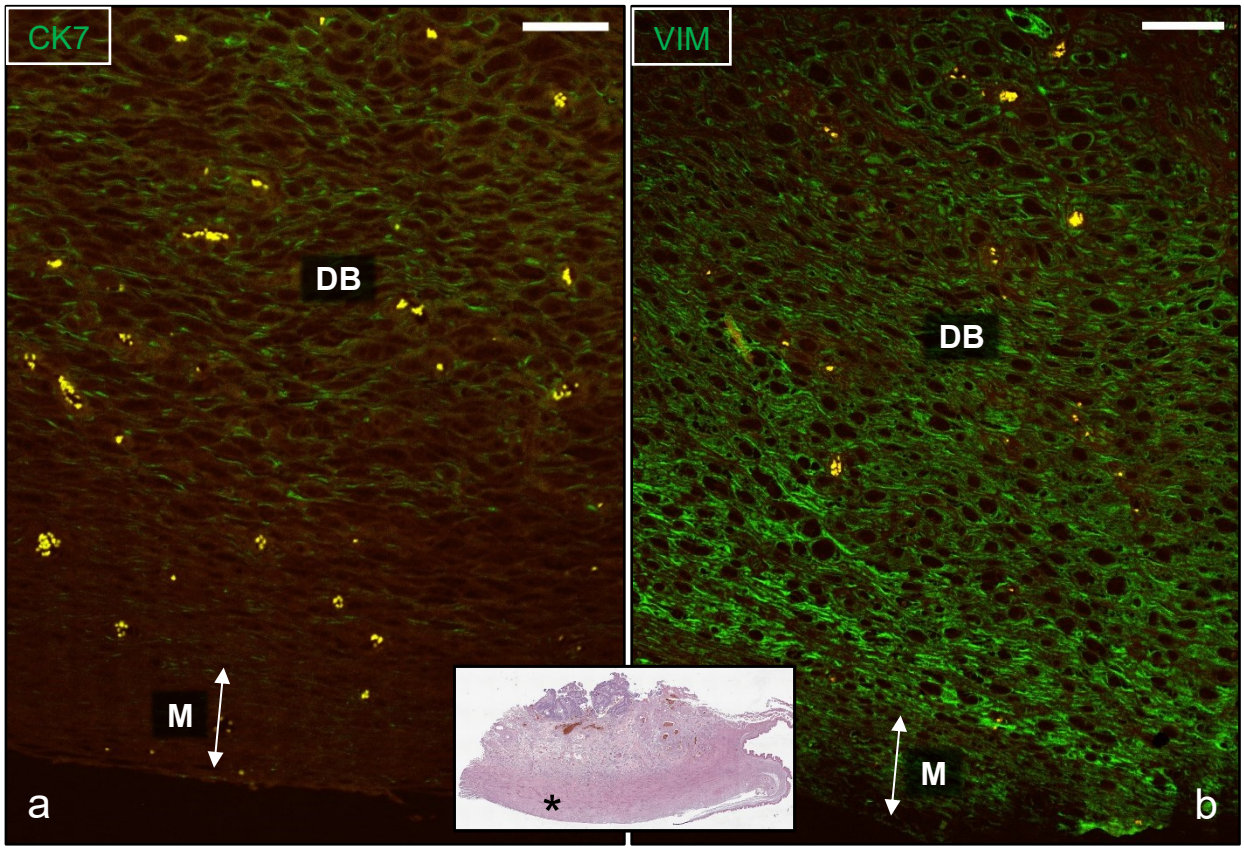

Figure 11 *myometrium (M) to decidua basalis (DB) at* ***30.5 dpc****, the irregularly shaped decidual cells with wide perinuclear space (dark circles in the tissue) are more prominent than the compact myometrial cells. Scale bar: 100µm. (signal: green; autofluorescence: yellow)*
a) a fraction of decidual cells, but no myometrial cells show immunoreactivity to CK7. IHC for CK7.
b) vimentin-expression appears in high intensity within the decidua basalis and low intensity in the myometrium. IHC for VIM.

A further approach to distinguish these strata involves examining the morphology of the smooth muscle cells in the myometrium and the cellular composition of the decidua. The shape of the muscle cells is elongated and narrow and they are small in size. The size of decidual cells enlarges as they progress towards the junctional zone (JZ), accompanied by a wider perinuclear space and, consequently, a diminished cytoplasmic volume.

The decidua basalis contains decidual stromal cells, maternal blood vessels, and immune cells. According to Davies, Dempsey, & Amoroso (1961) the decidual layer transitions from the myometrium towards the foetus through decidual giant cells (DGC) into the so-called junctional zone. It has been suggested that the giant cells are derived from hypertrophy of decidual cells. They are characterized by the variable appearance (pleomorphism) of their nuclei and their cytoplasm with ground-glass appearance. Our material does not provide definite evidence for the presence of decidual giant cells, as they have no affinity to most dyes. Moreover, neither VIM- nor CK-antibodies have a different expression in normal and giant decidual cells. Both types of decidual cells are individually encapsulated by PAS positive material, appearing as a pink stain (see Fig.12). Additionally, in comparing the PAS stains with amylase and with distilled water, we can observe indications for the presence of a carbohydrate distinct from glycogen as the amylase treatment (digesting glycogen) did not affect the capsule. Cytoplasmic materials of the DGC, like glycogen, are released into the junctional zone while degenerating (Davies, Dempsey, & Amoroso, 1961).

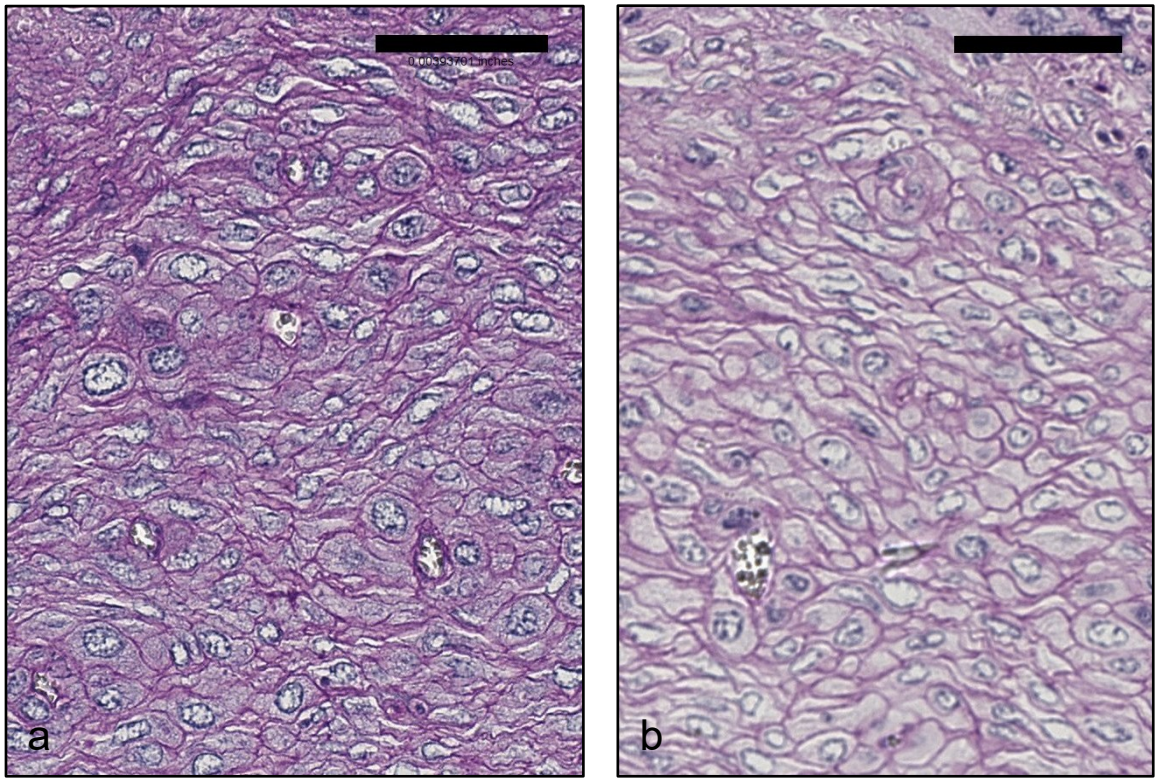

Figure 12 *neighboring sections of decidual stromal cells of guinea pig decidua basalis at* ***30.5 dpc****.*
Scale bar: 100 µm.
a) the tissue was treated with distilled water and PAS stain, resulting in pink dyed carbohydrates; they are present in the cytoplasm and cell membrane of decidual cells in variable concentrations. PAS.
b) the tissue treated with amylase and PAS stain reveal that the capsules of decidual cells contain carbohydrates other than glycogen as the pink color remains; the cytoplasm is colorless, which means that the glycogen was digested by the amylase treatment. PAS-D.

Spatially adjacent to the DGC and emerging from the subplacental cytotrophoblastic layers (CY), are the trophoblast giant cells (TGC). They invade the junctional zone, disintegrate at the margin to the decidua basalis and make this area acidic due to the released nuclear components. Consequently, this zone appears more purple in H&E staining compared to other layers, which is attributed to the binding of the basic dye haematoxylin by acidic cell material. The TGC have many small even sized nuclei with a fine granular cytoplasm and a variable amount of glycogen. They are distinguishable from the other cells and debris by their purple granular appearance in H&E staining and their cytokeratin-immunoreactivity, as seen in Figure 13a-b.

Davies, Dempsey, & Amoroso (1961) stated that the junctional zone is similar to the human placental basal plate. The latter consists of decidua, fibrinoid (including basic ECM, fibrin, immunocytes and dead trophoblast cells), connective tissue, extra-villous trophoblast and maternal vessels (Richani, et al., 2007). Indeed, we find a similar composition of the guinea pig junctional zone. In humans, cytotrophoblastic cell columns yield extra-villous trophoblast cells that invade the FMI. In guinea pigs, we find comparable extra-villous-like trophoblasts proliferating from stem cell aggregations of the subplacenta (SP) throughout the junctional zone (Mess, Zaki, Kadyrov, Korr, & Kaufmann, 2007). These extra-placental trophoblastic cells (EPTC) are limited to the junctional zone and are detectable through their cytokeratin expression (see Fig.13b & d). Further fetal structures within the fetal-maternal interface include syncytial streamers (SYN), which emerge from the subplacental trophoblast and move through the junctional zone. These invasive streamers are vacuolated to variable degrees and have an elongated appearance (see Fig.13b & d). All three types of trophoblasts, the TGCs, the invasive syncytiotrophoblast streamers and the extra-placental trophoblast cells reach to the margin of the decidua but seem to not penetrate it. They have their maximum invasive and proliferating activity during the implantation period and are on the wane again after 25 days in gestation (Davies, Dempsey, & Amoroso, 1961). On 30.5 dpc, they are still recognizably present. The most invasive activity of trophoblast cells within the fetal-maternal interface occurs in proximity to the subplacenta, as evidenced by the accumulation of trophoblastic structures in this area.

From apoptotic and necrotic decidual and trophoblast cells (Kliman, et al., 2012; Straszewski-Chavez, Abrahams, & Mor, 2005) arise the remarkable amorphous masses of the junctional zone (see Fig.13a-c). Similar as in the human basal plate, these are fibrinoid structures, containing basic ECM, immune cells, fibrin and dead cells. In addition to the amorphous masses, necrotic vesicles form with a varying number of nuclei. They are neither cytokeratin- nor vimentin-positive but eosinophil, which shows as their basic components strongly bind to acidic eosin, appearing

pink in H&E staining (see Fig.13a). Amid the cellular debris and trophoblast cells of the junctional zone, mesenchymal, decidual and vascular endothelial cells are present. As depicted in Figure 13c, these cells have intense vimentin-immunoreactivity.

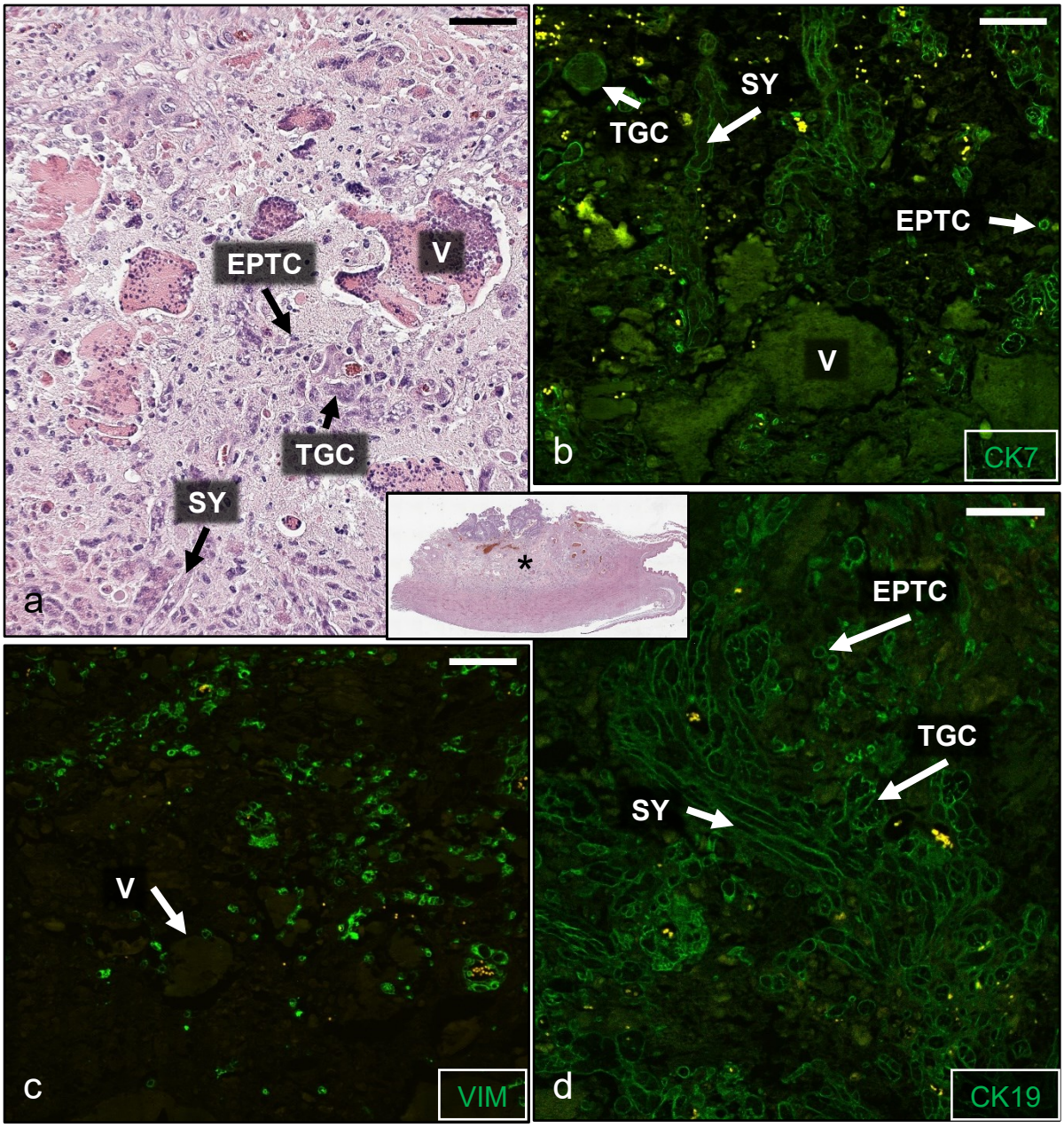

Figure 13 *junctional zone of the fetal-maternal interface in guinea pig at* ***30.5 dpc****, consisting of fibrinoid, trophoblasts, decidua, and blood vessels. Scale bar: 100 µm. (signal: green; autofluorescence: yellow)*
a) basic necrotic vesicles (V) appear pink as acidic eosin binds, they contain nuclei in varying numbers; extra-cellular space consists of fibrin and cellular debris; trophoblastic cells are purple-stained, because of the binding hematoxylin; extra-placental trophoblast cells (EPTC) and trophoblastic giant cells (TGC) are distinguishable in size, and syncytial streamer (SY) in their vacuolated and elongated appearance. H&E.
b) syncytial streamer, EPTC and TGC are CK7-positive and distinguishable in morphology. IHC for CK7.
c) decidual cells, fibroblasts/mesenchymal cells and endothelial cells show vimentin-immunoreactivity; towards the subplacenta (top) the concentration of VIM-positive cells increases. IHC for VIM.
d) all three types of trophoblasts in the junctional zone are CK19-positive. IHC for CK19.

Maternal vessels traversing the junctional zone extend through the lateral subplacenta to supply the chorio-allantoic placenta. The replacement of endothelium within the maternal vessel walls by extra-placental trophoblast cells begins early in gestation. These trophoblast cells are intensely cytokeratin-immunoreactive (see Fig. 14a). Notably, at 30.5 dpc, trophoblast cells are still interspersed with endothelial cells of maternal arteries (MA). The remaining endothelium, decidual cells and fibroblasts demonstrate vimentin-positivity, as depicted in Figure 14b.

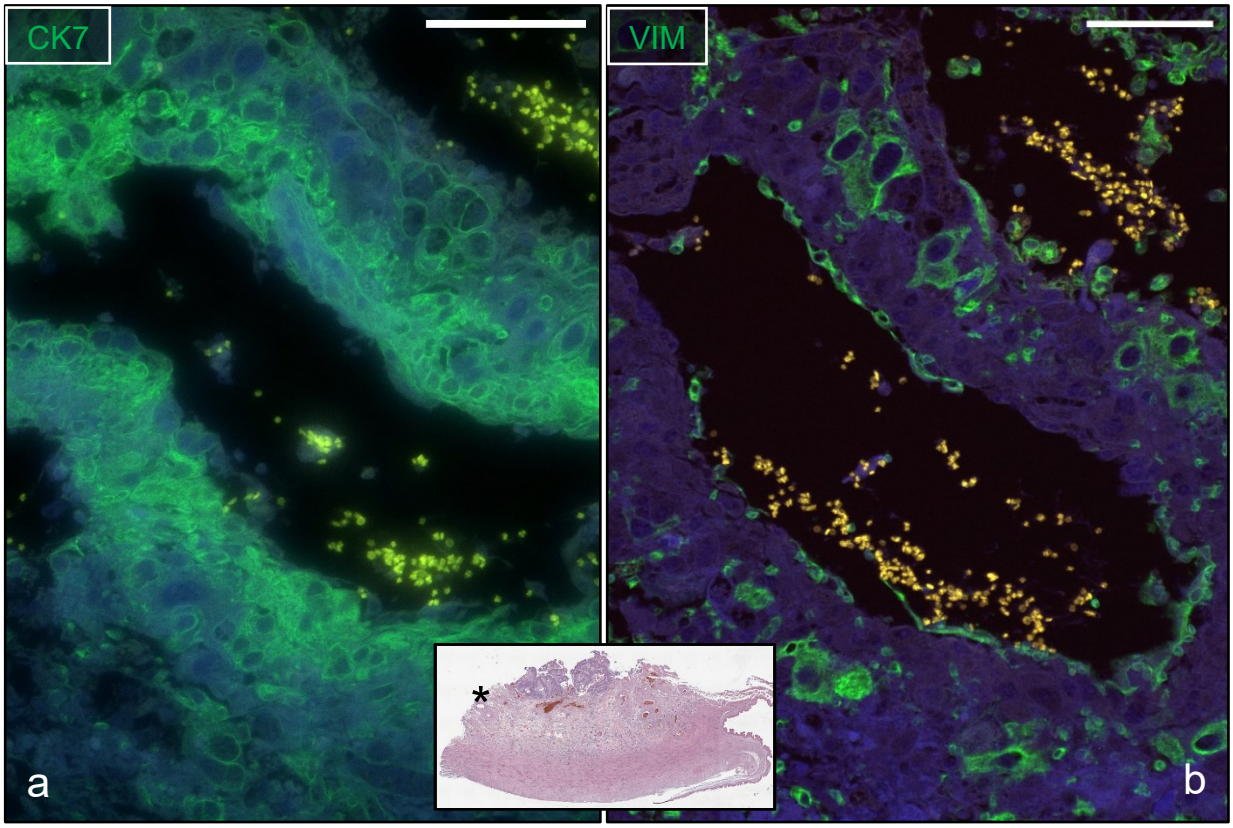

Figure 14 *a maternal artery within the junctional zone of guinea pig at* ***30.5 dpc****, neighboring sections.*
Scale bar: 100 µm. (signal: green; autofluorescence: yellow; background: yellow)
a) arteries are surrounded by invasive CK7-positive extra-placental trophoblast cells. IHC for CK7.
b) some remaining VIM-positive endothelium lines the maternal artery, decidual cells and mesenchymal cells/fibroblasts in surrounding area are also immunoreactive against anti-vimentin. IHC for VIM.

The subplacenta originates from a part of the chorion, which undergoes differentiation between 15 and 16 days post copulation (Davies, Dempsey, & Amoroso, 1961). Later in gestation, the subplacenta is situated between placental disc and junctional zone. When fully developed, it consists of multiple layers of cytotrophoblast forming an overall villous structure (see Fig.15). The subplacental syncytiotrophoblast, also known as syncytium (S), is produced through the division and fusion of cytotrophoblastic daughter cells. These daughter cells either form the syncytium pervaded by fetal capillaries within the cytotrophoblastic layers, or they transform into syncytial streamers and trophoblastic giant cells migrating towards the decidua basalis.

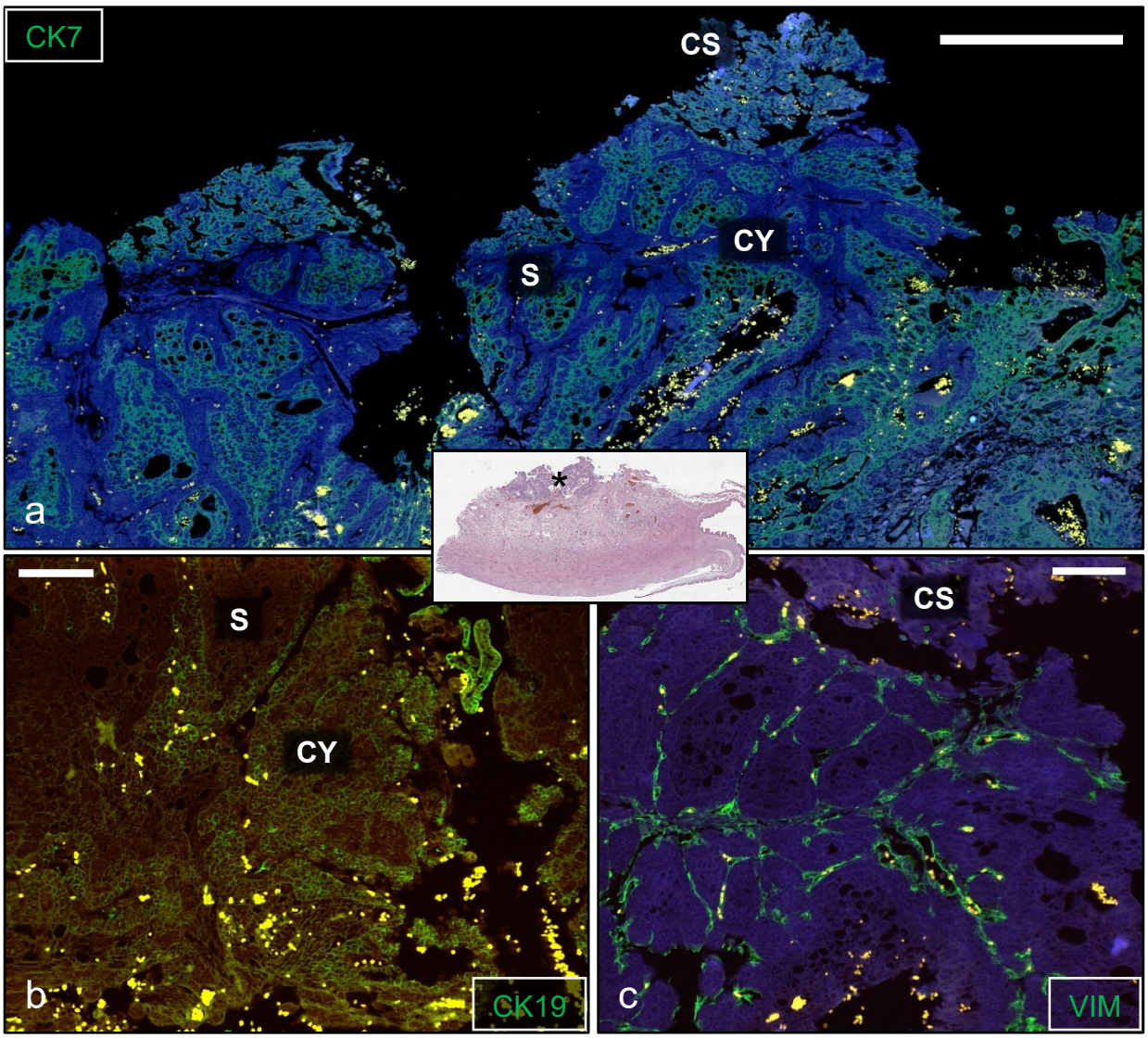

Figure 15 *the subplacenta of guinea pig at* ***30.5 dpc****, consisting of cytotrophoblastic (CY) layers and syncytium (S) in-between; the whole structure is situated between junctional zone and here removed chorio-allantoic placenta. (signal: green; autofluorescence: yellow; background: blue in a, c and red in b)*
a) subplacental syncytium and the coarse syncytium (CS) of chorio-allantoic placenta are CK7-positive. IHC for CK7. Scale bar: 500 µm.
b) subplacental cytotrophoblast is CK19-immunoreactive. IHC for CK19. Scale bar: 100 µm.
c) mesenchymal and endothelial cells are VIM-positive. IHC for VIM. Scale bar: 100 µm.

A similar process to the decrease in trophoblastic cell number observed in the decidua also occurs in the subplacenta. First, the cytotrophoblast layers increase and augment in complexity, followed by a subsequent decrease after day 25. The subplacental syncytium changes from overall highly vacuolated in early gestation, to more vacuolated syncytium towards decidua and margin of the subplacenta (Davies, Dempsey, & Amoroso, 1961), to an even distribution of compact and vacuolated syncytium in mid to late gestation. Between day 25 and 45 the production of syncytiotrophoblast by the cytotrophoblast is at its maximum, resulting in a progressive

compaction of syncytium towards term and a thinning of the cytotrophoblastic lamellae (Davies, Dempsey, & Amoroso, 1961). Therefore, in our tissue samples at 30.5 dpc, we find an evenly compact and vacuolated subplacental syncytium within multi- to one-layered cytotrophoblast.

Sections incubated with cytokeratin7-antibody reveal the subplacental syncytium, but not the cytotrophoblast (see Fig.15a). Interestingly, the opposite case applies to the CK19-immunoreaction. In Figure 15b we can observe cytokeratin19-positive cytotrophoblasts and -negative syncytium. Such a distinction is not observable in trophoblasts of the junctional zone. Vimentin-positive cells are present as the mesenchymal septa between the cytotrophoblast and the endothelium of fetal vessels (FV), as depicted in Figure 15c.

Syncytial trophoblast and the trophoblast cells eroding the endothelium of maternal vessels show PAS positive droplets (see Fig.16), indicating that these cells are rich in glycogen. In contrast, the cytotrophoblast cells are PAS negative. Its nuclei are acidic, binding the basic hematoxylin in H&E and PAS staining. This basophilia is also showing in nuclei of syncytial trophoblast and in the perinuclear zone of the chorionic giant cells (CGC), as depicted in Figures 16 and 17b.

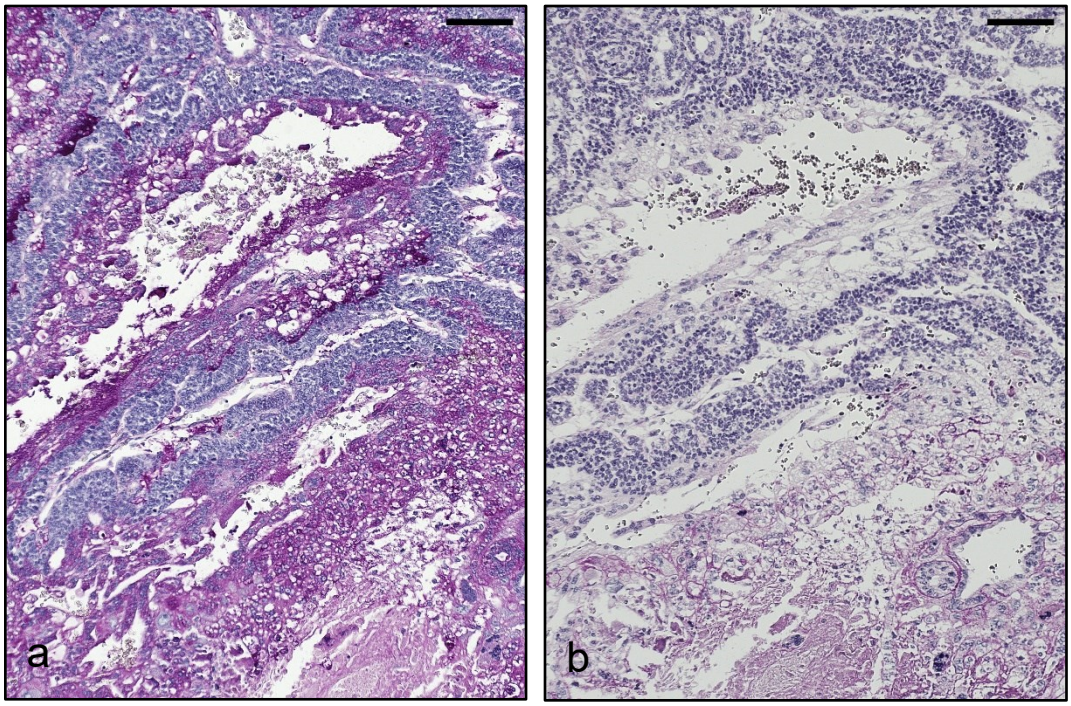

Figure 16 *guinea pig subplacenta at* ***30.5 dpc****; neighboring sections. Scale bar: 100 µm.*
a) tissue treated with PAS stain and distilled water appears in dark pink, that includes subplacental syncytiotrophoblast and trophoblasts lining maternal blood vessels; cytotrophoblasts are not stained, indicating the absence of glycogen in these cells, due to hematoxylin its cell nuclei appear purple. PAS.
b) tissue subjected to PAS stain and amylase treatment shows a colorless subplacental syncytiotrophoblast and trophoblast in vessel walls, indicating the digestion of their glycogen content; the cytotrophoblastic layers are still recognizable by their purple-stained nuclei. PAS-D.

These giant cells accumulate at the lateral junction of chorio-allantoic placenta and subplacenta and have a different morphology compared to the trophoblastic giant cells within the junctional zone. The cytoplasm of CGC is less acidic and appears pink in H&E staining (see Fig.17b). They are always uninucleate and have a wide perinuclear space. The layer of chorionic giant cells is connected to the parietal endoderm (PE), which surrounds the chorio-allantoic placenta, and terminates at the margin of the subplacenta adjacent to the junctional zone (see Fig.17a). This yolk sac wall is a pseudo-stratified columnar epithelium delineating the lateral main placenta, stopping at the visceral yolk sac (VYS) membrane and at the chorio-decidual junction. Both structures, the parietal wall of the yolk sac and chorionic giant cells, are well developed between day 20 and 45 (Davies, Dempsey, & Amoroso, 1961). The CGC have a low immunoreaction to anti-cytokeratin and the parietal endoderm is strongly vimentin-positive (see Fig.17a, c).

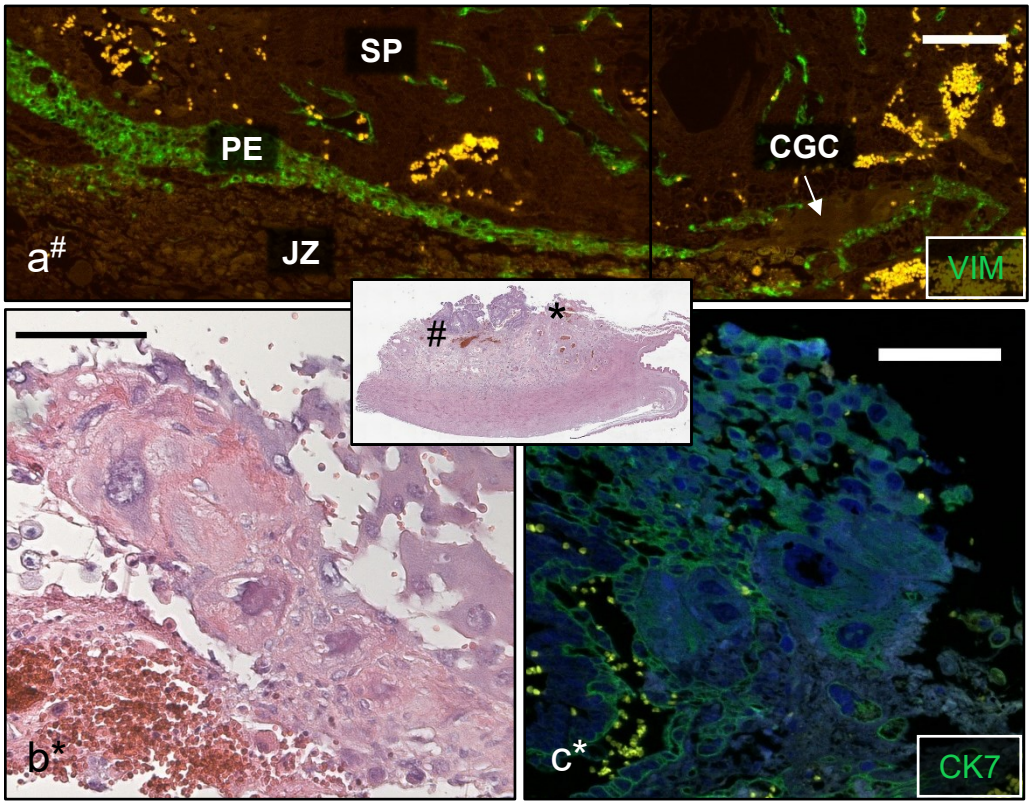

Figure 17 *chorionic giant cells (CGC) lateral to the guinea pig subplacenta (SP) and connected to a layer of parietal endoderm at* ***30.5 dpc****; the small image provides an overview for the location of the sections in a, b and c. Scale bar: 100 µm. (signal: green; autofluorescence: yellow; background: red in a, blue in c)*
a) parietal endoderm (PE), and endothelial cells and mesenchymal cells of the subplacenta are VIM-positive; CGC and amorphous material of junctional zone (JZ) are not immunoreactive. IHC for VIM.
b) eosinophil chorionic giant cells appear pinkish due to their basic cytoplasm reacting with acidic eosin; acidic perinuclear space and nuclei are stained purple with basic hematoxylin. H&E.
c) cytoplasm of CGC is immunoreactive to CK7, as are the surrounding trophoblast cells. IHC for CK7.

Additionally, on the lateral site, where subplacental syncytium encounters the syncytium of the main placenta, we observe an irregular intensely acidic intermediate zone (IZ), which shows in H&E staining as pinkish to purple cells (see Fig. 18). This zone is formed by condensation and fusion of syncytial nuclei and ends at the region where chorionic giant cells accumulate.

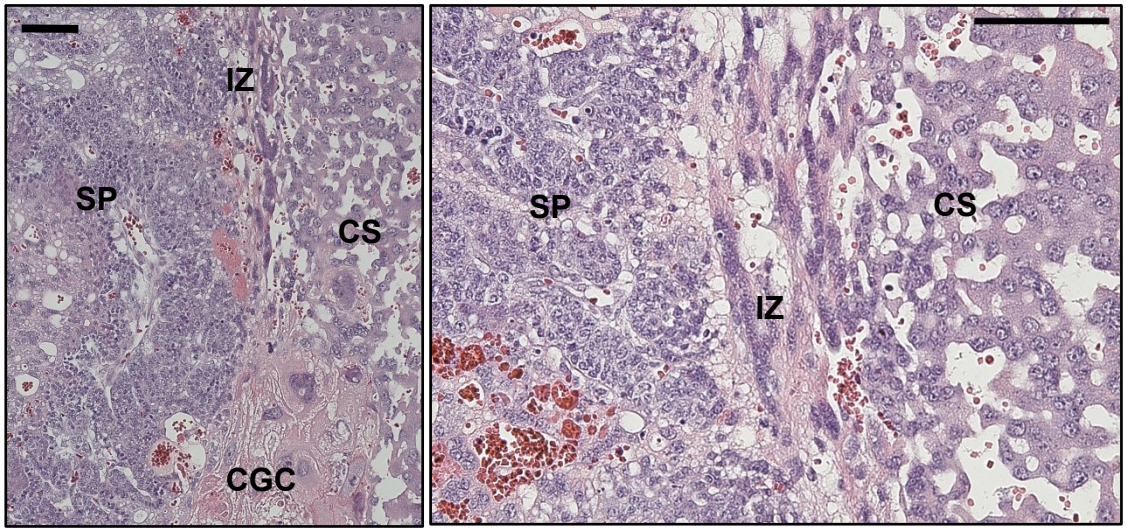

Figure 18 *intermediate zone (IZ) in guinea pig at* ***30.5 dpc****; situated between coarse syncytium (CS) of chorio-allantoic placenta and subplacental (SP) cytotrophoblastic layers, emanating from chorionic giant cells (CGC) towards fetal tissue; in H&E staining, the cells of the intermediate zone appear in varying pink and purple colors. H&E. Scale bar: 100 µm.*

A plane of fetal mesenchyme is separating the main placenta and subplacenta proximal. Fetal and maternal vessels are carried through this mesenchymal plane. Maternal vessels traverse through the subplacenta and open into blood spaces of the main placenta, where they are restrained by syncytium. As the chorio-allantoic placenta is not in our tissue samples of 30.5 dpc it is described in more detail at 55 dpc.

5.4. The fetal-maternal interface at late gestation (55 dpc)

The chorio-allantoic placenta (shown in Fig. 19) finds its mature form between 30 and 35 dpc and remains in this form until close to term (Carter, Tanswell, Thompson, & Han, 1998). The distinctive arrangement of the subplacenta is no longer discernible by the time it reaches 55 days post-conception.

In contrast to the subplacenta, the main placenta exclusively comprises syncytial trophoblast throughout pregnancy. The syncytium forms an interlobular network enabling the passage of maternal and fetal blood without direct contact. Due to the hemomonochorial placentation, a single layer of syncytium separates maternal blood from fetal vascular endothelium. Maternal blood freely circulates within the lacunae of the placenta. The syncytium, shown in Figure 19 and

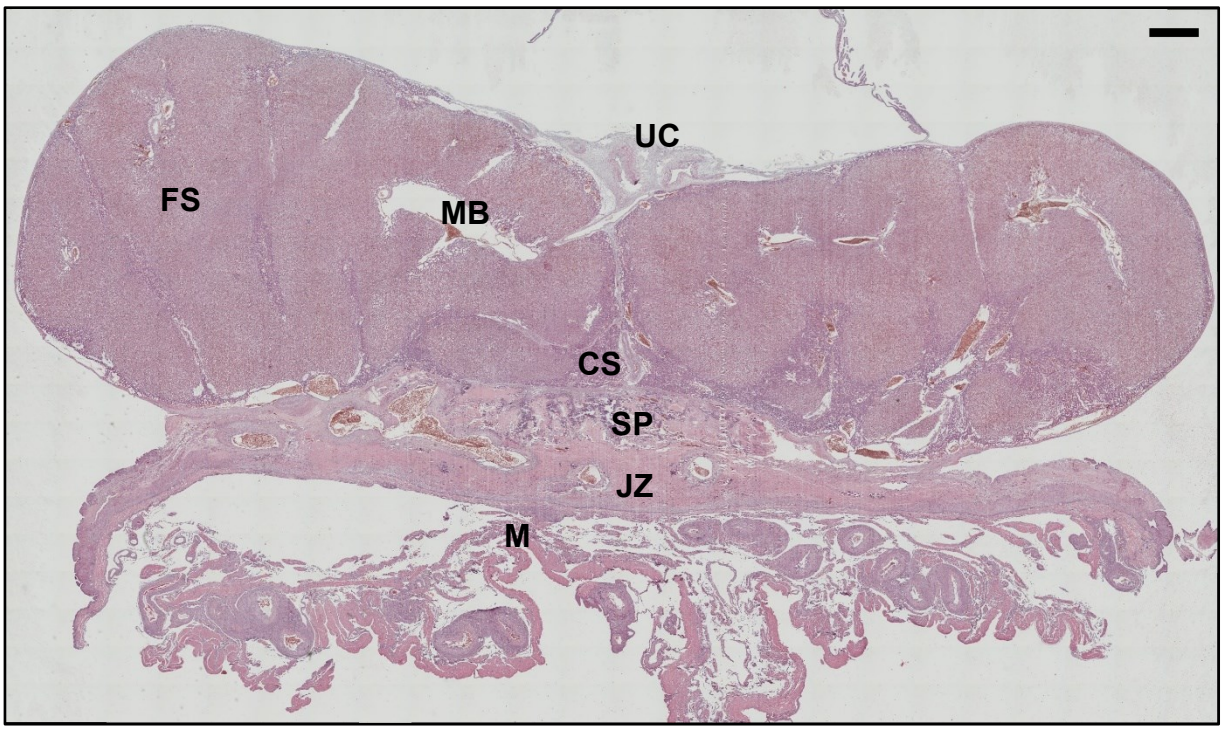

Figure 19 *longitudinal tissue section of* ***55 days*** *pregnant guinea pig, overview for the later in detailed described areas; myometrium (M), junctional zone (JZ), subplacenta (SP) and chorio-allantoic placenta consisting of fine (FS) and coarse syncytium (CS); maternal blood spaces (MB) are prominent within the labyrinth and FMI; the umbilical cord (UC) is partly implied at the top of the main placenta. H&E. Scale bar: 1000 µm.*

20, is further differentiated into a fine syncytium (FS), characterized by numerous small and narrow blood channels and vessels, and a coarse syncytium (CS) with fewer but larger channels and vessels. The maternal blood sinuses have no endothelium and basement membrane and are surrounded by cytokeratin-positive syncytium (see Fig.20a) while the newly build fetal capillaries have a vimentin-positive endothelium resting on a basement membrane (see Fig. 20b). The maternal blood spaces (MB) are recognizable in their great size and fuzzy outline. They are passageways for the maternal blood, therefore not tube-like. We find them in the fine and coarse syncytium, which are both cytokeratin7-immunoreactive. On the contrary, we cannot observe fetal capillaries in the coarse syncytium but larger fetal vessels, recognizable by their vimentin-positive endothelium.

The mesenchymal plane, separating the two placental structures, proceeds through the centre of the chorio-allantoic placenta up to the umbilical cord (UC). In Figure 20b, the fetal mesenchyme is recognizable due to the strong VIM-immunoreactivity.

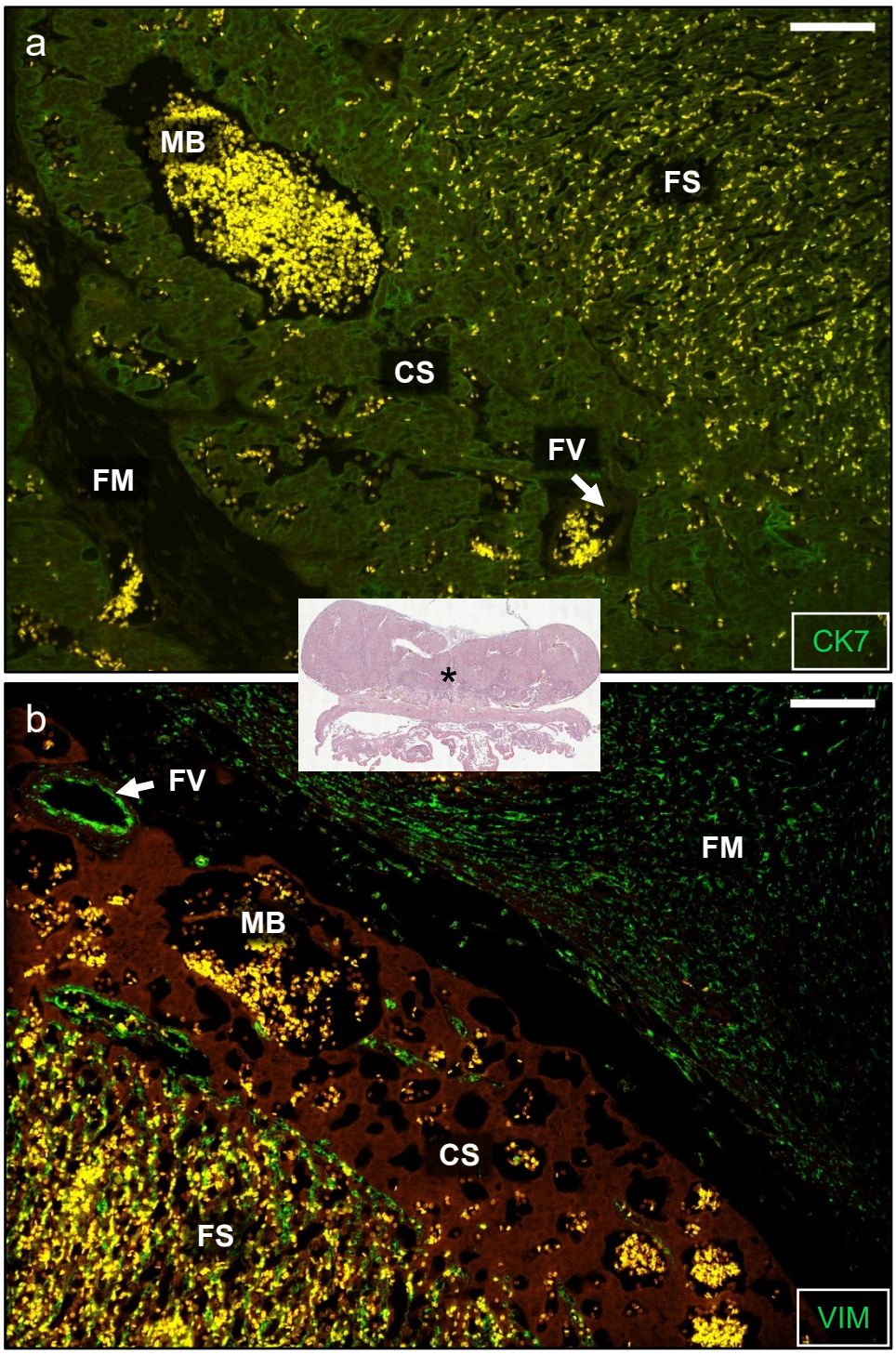

Figure 20 *sections of the chorio-allantoic placenta of guinea pig at* ***55 dpc****; maternal blood sinuses (MB) and fetal vessels (FV) are within the coarse syncytium (CS); the fine syncytium (FS) is pervaded by erythrocytes and endothelium of fetal capillaries; fetal mesenchyme (FM) traverses the center of the placenta towards the umbilical cord. Scale bar: 100 µm. (signal: green; autofluorescence: yellow)*
a) both syncytial structures of the main placenta are CK7-positive. IHC for CK7.
b) fetal mesenchyme and the endothelium of fetal vessels and capillaries are vimentin-immunoreactive. IHC for VIM.

The parietal endoderm and chorionic giant cells line the lateral sides of the chorio-allantoic placenta towards the decidual cavity. The cell layers of the parietal endoderm consist of mesenchymal cells (VIM+) covered by cytokeratin-positive surface columnar epithelium of the parietal yolk sac (see Fig.21). These layers are organized in a villous structure. The placental wall progressively diminishes to one layer of cellular connective tissue at term. On 55 dpc we can observe a thinned CGC layer and a non-villous parietal endoderm. Towards subplacenta both structures fade.

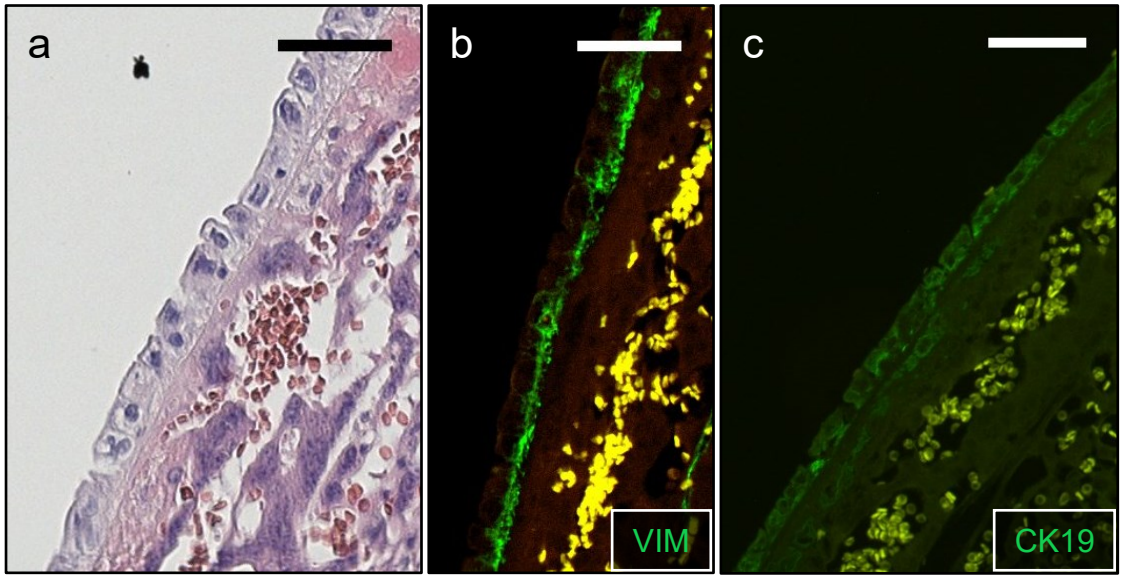

Figure 21 *the placental wall at* ***55 dpc*** *consisting of parietal yolk sac epithelium, mesenchymal cells and CGC; the wall rests on coarse syncytium. Scale bar: 50 µm. (signal: green; autofluorescence: yellow)*
a) coarse syncytium in dark purple, components of the placental wall appear in light purple. H&E.
b) mesenchymal cells of placental wall visible due to VIM-immunoreaction. IHC for VIM.
c) detectable signal of CK19 in epithelial cells and residual CGC of placental wall. IHC for CK19.

The previously by Davies, Dempsey, & Amoroso (1961) described degradation of the subplacenta from day 45 in gestation is well advanced in our tissue sample at day 55 (see Fig.22). The multi-layered continuous cytotrophoblast progressively loses layers and becomes discontinuous. It is still immunoreactive against CK19 (see Fig.22b) and surrounded by some cytokeratin7-positive syncytium (see Fig.22a). The space previously occupied by the subplacenta is now filled with acidophilic amorphous material and resembles the structure of the junctional zone at mid gestation. Trophoblast migration, increase in ECM and programmed cell death lead to a morphological shift away from the characteristic lamellar structure. The mesenchymal and endothelial cells between the cytotrophoblastic remains are sparse and scattered and can be identified through their anti-vimentin immunoreaction (see Fig.22c). Merely the vessels within the subplacenta seem unaltered, maintaining their elongated appearance.

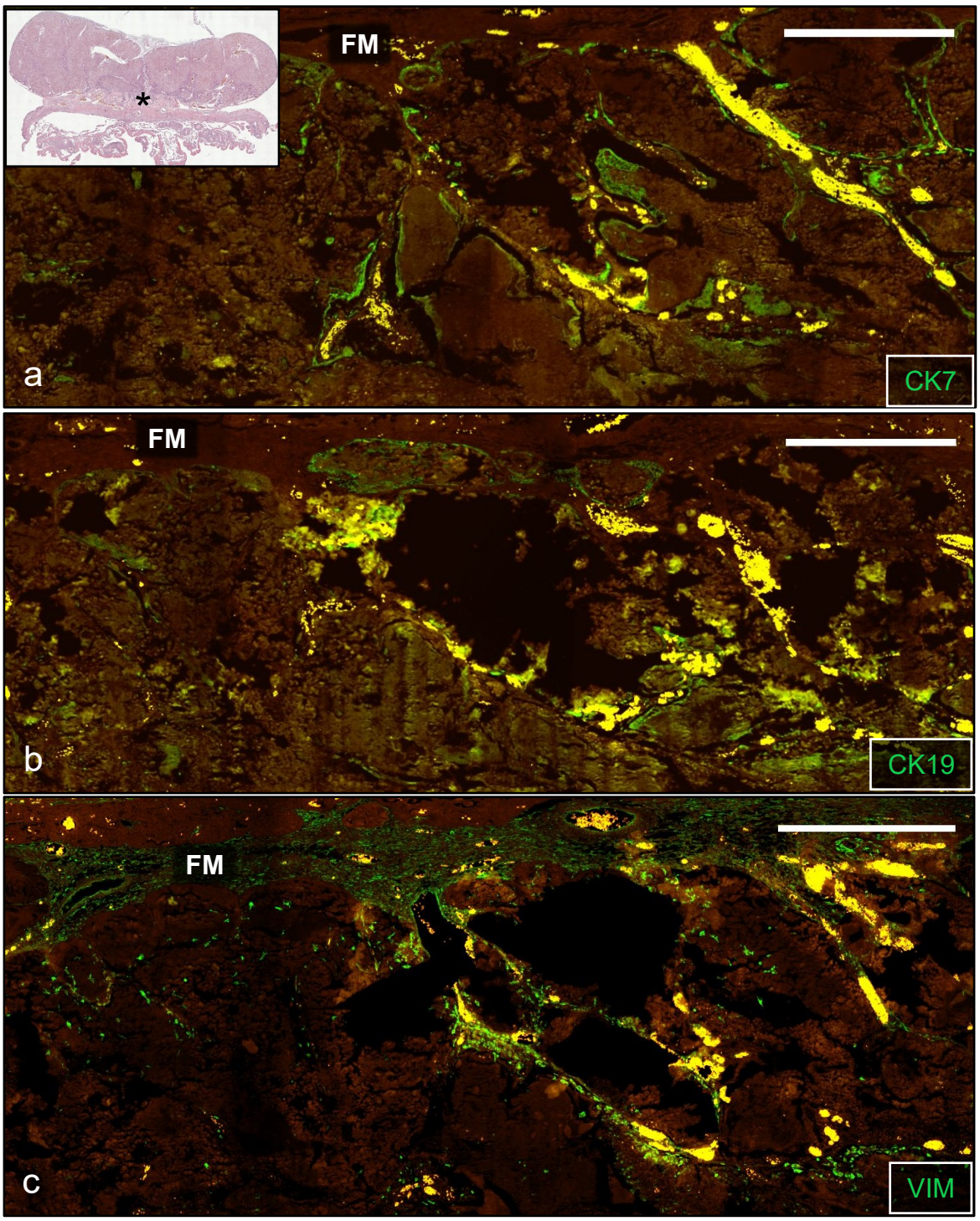

Figure 22 *sections of the guinea pig subplacental apoptotic/necrotic masses at* ***55 dpc****; they are pervaded by blood vessels and a plane of fetal mesenchyme (FM) lies between the masses and the chorio-allantoic placenta. Scale bar: 500 µm. (signal: green; autofluorescence: yellow)*
a) degrading syncytial trophoblast appears CK7-immunoreactive, mainly situated in proximity to the blood vessels; fetal mesenchyme (FM) and necrotic masses are non-CK7-immunoreactive. IHC for CK7.
b) residual cytotrophoblast reacts with CK19, FM and necrotic masses express no signal. IHC for CK19.
c) fetal mesenchyme between chorio-allantoic placenta and subplacenta is strongly vimentin-positive, as are the endothelial and mesenchymal cells of the degrading subplacenta. IHC for VIM.

The junctional zone at 55 dpc appears as a homogenous acidophilic mass in a pinkish colour in H&E staining, as shown in Figure 23c. Necrotic vesicles, observed within the junctional zone at mid gestation, are no longer identifiable at late gestation. Moreover, extra-placental trophoblast

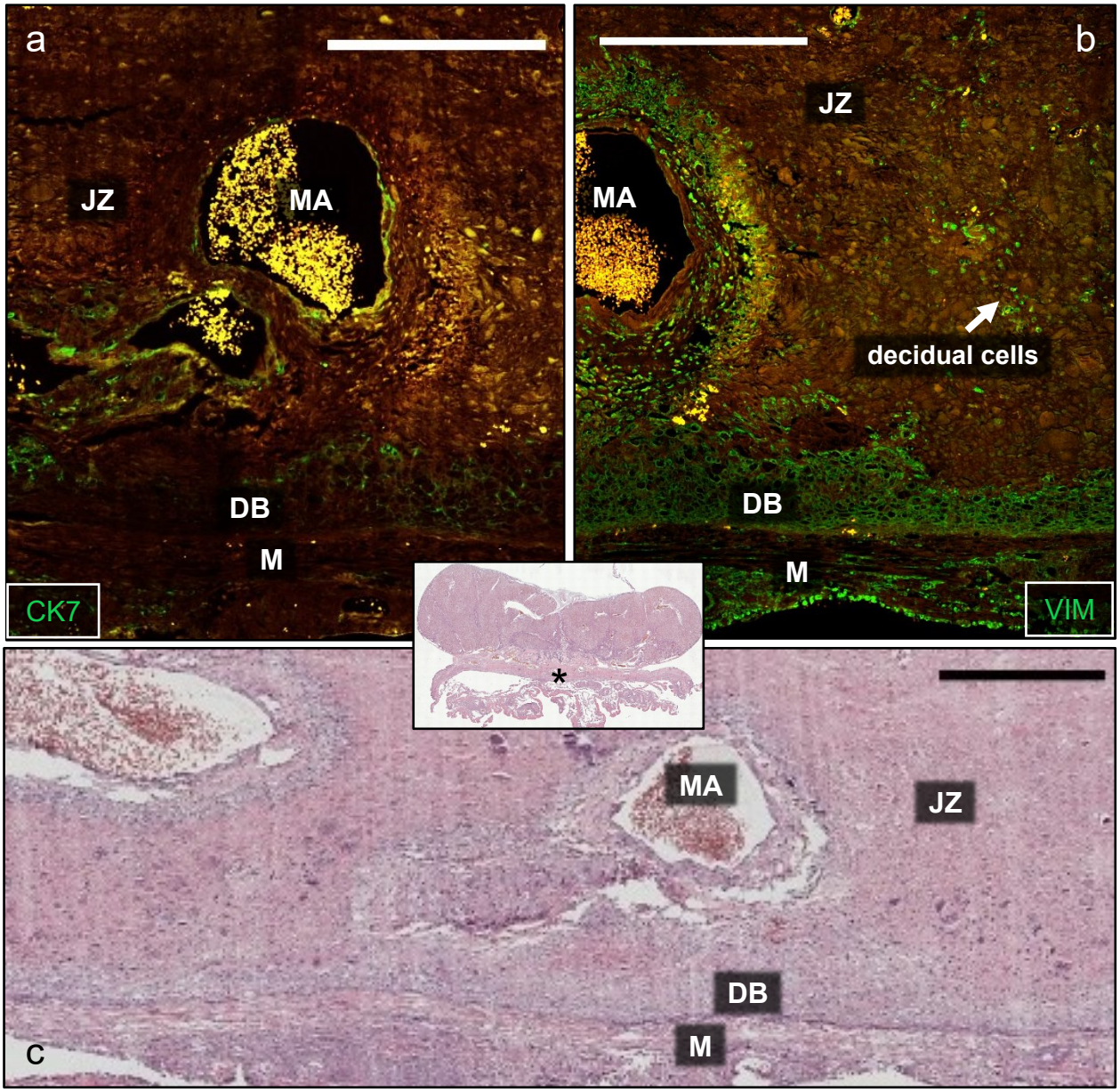

Figure 23 *the guinea pig junctional zone (JZ), decidua basalis (DB) and myometrium (M) at* ***55 dpc****. Scale bar: 500 µm. (signal: green; autofluorescence: yellow)*
a) maternal arteries (MA) are lined with a thin layer of CK7-positive trophoblast and individual EPTC within vessel walls; cells of the decidua basalis, remaining extra-placental trophoblast cells and trophoblastic giant cells within the junctional zone express cytokeratin7. IHC for CK7.
b) decidual cells within the junctional zone and numerous fibroblasts surrounding the maternal arteries are vimentin-positive; the decidua basalis exhibits strong vimentin-immunoreactivity; within the myometrium we observe endothelial cells and fibroblasts that are vimentin-positive. IHC for VIM.
c) the junctional zone mainly occupied by eosinophil masses, appears in pink color, with basophil trophoblastic structures scattered throughout the zone, observable in purple color. H&E.

cells and trophoblastic giant cells have significantly decreased in number, while syncytial streamer are absent in our 55 dpc samples. Individual EPTC are situated alongside the TGC at the junctional-decidual border, yet they predominantly accumulate within vascular walls (see Fig. 23a). Maternal arteries and vessels of the junctional zone are completely trophoblast-lined (CK+) with abundant fibroblasts (VIM+) within the vessel walls (see Fig.23a-b). A significant number of decidual cells, both those still active and that undergoing necrosis, persist in abundance. The cells are distributed among the amorphous masses in the junctional zone, and they exhibit anti-vimentin signal (see Fig.23b).

The cells of decidua basalis persist in close association with trophoblast cells at the junctional-decidual border, displaying a more acidic cytoplasm (light purple in H&E staining, as depicted in Fig.23c) compared to mid gestation. The decidual layer appears stretched and thinned, resting atop the inner myometrium. Decidua and myometrium are separated by a strongly acidic border, showing as a dark purple line in H&E staining. Additionally, both layers are distinguishable through the VIM-immunoreactivity of decidual cells and non-reactivity of smooth muscle cells. In our sections of 55 dpc the known organization of the myometrium remains intact. We can observe a loose outer myometrial layer surrounding the vascular layer that delineates the inner myometrium.

6. Discussion

In this study, we aimed to explore the morphological changes in the guinea pig uterus during implantation (6.5dpc), and mid (30.5dpc) to late (55 dpc) gestation and compare these to non-pregnant diestrus stage. The primary objective of this investigation was to delineate the variations in cell composition and tissue structure in the guinea pig uterus across different reproductive states. To decipher the general fetal-maternal interface of guinea pig gestation, we first distinguished between maternal and fetal tissues using immunohistochemistry for trophoblast marker cytokeratin7 and a maternal decidual fibroblast marker, Vimentin. The subsequent steps expanded the cellular detail by including further marker proteins, to determine the distribution of other epithelial cells (IHC for cytokeratin19), or immune and/or endothelial cells (in situ for Pecam1), as well as regions of increased proliferation (marked by Ki67). Detail was also enhanced by using classical histological tools such as staining for glycogen and collagen. The cytokeratin 7 and 19, vimentin and Ki67 antibodies were raised against mice, therefore our results demonstrate cross-reactivity across mouse and guinea pig reproductive tissue. Additionally, further histological stainings and the in-situ staining (RNAscope™) were positive.

The non-pregnant (diestrus) stage served as a reference point, providing context and guiding comparisons with other stages. Given the generally brief implantation window, between days 6 and 7 post copulation (Enders & Schlafke, 1969), “implantation” samples collected at 6.5 dpc may contain blastocysts, either attached or not attached. Upon examination, our implantation samples were identified as either in preimplantation phase or indicative of unsuccessful blastocyst development. In the epithelial and stromal cells surrounding possible attachment sites of a blastocyst, no characteristic modifications were observed. The embryo-related cell mass could not be definitively identified as a blastocyst. Nonetheless, as we did find distinct changes, we refer to the samples henceforth as the implantation stage. The mid gestational sections yielded intriguing insights into the gestational tissues, as they revealed significant transformations in the fetal-maternal interface, characterized by differentiation of stromal fibroblast into decidual secretory cells, necrotic and apoptotic processes and reaching the maximum development of the subplacenta. Late gestational samples revealed the progress of apoptosis and necrosis occurring during gestation and manifesting the fully developed state of the chorio-allantoic placenta.

6.1. Histological comparison of guinea pig uterus at implantation relative to diestrus

The non-pregnant guinea pig uterus represents the general structure of a rodent uterus (Wooding & Burton, 2008). The semi-continuous uterine lumen is enclosed by endometrium filled with

tubular glands, which is surrounded by the two-layered myometrium. The layers consist of longitudinal and circumferential muscle fiber bundles intervened by a vascular layer. Among the three embedded samples of uterine horn dissected at implantation stage we observed only one embryo-related cell cluster. However, also in this sample, we observed no clear signs of decidualization or any other fetal tissue. The identified cell compositions comprise identical cell types in the implantation uterus, as in the non-pregnant one.

Observable changes include the decrease of collagen density on the mesometrial side of the uterine horn at 6.5 dpc and the advanced closure of the uterine lumen. We proposed that these phenomena are attributed to the proliferation of stroma and the development of oedema. We detected proliferation (using IHC for Anti-Ki67) throughout the uterine horn in implantation uterus, as well as in luminal and gland epithelium, in the stroma and in vascular walls of the non-pregnant uterus. This implies that the increase in volume during the implantation phase is not exclusively caused by increased stromal proliferation, as this proliferation is shared in the two types of samples. Rather, the volume increase may also involve other processes, such as swelling of the uterine horns due to oedema. We also noted a change in gland size between stages. The uterine glands of the non-pregnant uterine horns are evenly large and build complex formations, whereas glands at 6.5 dpc are small and simple in structure. This probably indicates a decrease in gland activity at implantation which stands in contrast to the increased gland secretion during the later process of endometrial decidualization.

The distribution of immune cells (identified using RNAscope^{TM} for Pecam1), showed differences between the diestrus and implantation stage. In the non-pregnant uterus, they accumulate in the superficial stroma, either on the mesometrial or the anti-mesometrial side. In contrast, the immune cells are abundant in the myometrial layers and deep stroma of the implantation uterus, with fewer found in the superficial stroma. At both time points, progesterone levels are elevated, as in this phase the uterus prepares for (potential) pregnancy, followed by an increasing number of leukocytes. Progesterone influences the immune system, recruiting and activating various immune cells throughout the uterus. A possible explanation for this is a spread of inflammation processes required for implantation, from the uterine lumen to the entire uterus due to the detection of a blastocyst. While Pecam1 also labels endothelial cells, we can rule out distinct vascularization patterns or increases, as nothing of the sort was detected in other stainings.

The investigation of the implantation uterine horn for indicators of decidualization, as mentioned before, yielded no results. Using H&E staining, alternations in stromal fibroblast cell morphology were searched for, focusing on features such as enlargement, a shift towards a polygonal shape

and prominent nuclei, along the anti-mesometrial side of the uterine lumen. The observed cells resembled the spindle-shaped small fibroblast cells present in the non-pregnant uterus.

Overall, we could identify a composition of smooth muscle cells, pericytes, vascular endothelial cells, fibroblasts, immune cells, epithelial cells, and a limited number of mesothelial cells. We found that the increased volume during the implantation stage is not solely explained by an increase in proliferating stroma, and that it is accompanied by formation of oedema. We did not find an implanting blastocyst, apparent modifications in the luminal epithelium, nor signs of the onset of stromal decidualization.

6.1.1. Comparison of histology with single-cell RNA sequencing experiment

With the aid of single-cell RNA sequencing (scRNA-seq) data on the uteri of the same individuals, generated in the ongoing project in the lab Basanta & Stadtmauer (in prep.), we can verify our histological interpretation of cell types. The high-dimensional results of the scRNA-seq experiment are visualized in a two-dimensional UMAP. These maps show cell populations as clusters, reflecting similarity patterns present in the gene expression profiles of single cells. The two UMAP visualizations generated in this project show the cell populations of diestrus and implantation stage in uterine horns. Cell types in the project were derived through clustering, considering biological data and comparative analyses with other species (Basanta & Stadtmauer, in prep.).

Each of the major cell types found in histology is indeed identified based on the single cell transcriptome, with no differentiation observed between non-pregnant and implantation stage. The transcriptomic data differentiates found cell types into subpopulations; a heterogeneity not reflected in the histological phenotype. In the transcriptome, discrepancies were found in cell abundance between stages, with nearly all cell populations increasing in number at 6.5 dpc.

The amount of glandular and luminal epithelial cells increases significantly. This may appear contrary to the observation from the histological analysis, showing the luminal closure and reduced gland size. However, when considering the overall volume increase, this is likely a consequence of the overall increase in cell number. In the transcriptomic data, immunocytes also show a slight increase in number when comparing diestrus and implantation stage and could be specified as macrophages and natural killer cells. The fibroblasts found through histological analysis in the endometrium at both time points are subdivided into four subpopulations in the transcriptome. Among them, one subpopulation was identified as proliferating, exhibiting a significant increase at 6.5 dpc, a distinct proliferation not identified through histology. Lymphatic vessels, which are commonly present in the uterus at all time points and were identified through

scRNA-seq, were not recognized in histology. The advantage that the histological analysis brings is to be able to assign cell clusters found in scRNA-seq to specific areas within the uterine horns.

6.2. Histological analysis of guinea pig fetal-maternal interface at mid and late gestation

At 30.5 days in gestation, the myometrium in our samples appears denser and is indistinguishable from the by now modified endometrium. Decidualization of the endometrium is evident, resulting in changes of stromal fibroblast cell morphology and the absence of glands. The decidual layer contains decidual stromal cells, vascular endothelial cells, and a notable concentration of immune cells. Samples of 55 dpc display the same decidual composition, although the layer appears stretched and has a reduced width compared to the mid gestational sections.

Accurately identifying decidual giant cells poses a challenge, as all used stains target both types of decidual cells, and 2D morphology alone does not provide a clear indicator for distinction. In the junctional zone, maternal giant cells release their cellular contents into the space through necrotic processes. Within this junctional layer, maternal cells (decidual cells, artery-associated cells) encounter fetal cells (all types of trophoblasts), and both are distributed among necrotic and apoptotic masses. Cells in the junctional zone begin to undergo cell death from 16 dpc on (Davies, Dempsey, & Amoroso, 1961). Living cells are already a minority at 30.5 dpc and their presence is rare within the obscuring structures of the dead amorphous masses at 55 dpc. From the cell types present in the junctional zone at mid-gestation, such as decidual stromal cells, syncytial streamers, extra-placental trophoblast cells, and trophoblastic giant cells, only syncytial streamer were absent at late gestation. A reason for this observation lies in the apoptotic subplacenta during this gestational stage, where no new formation of trophoblast cells invading the junctional layer occurs. Moreover, the trophoblast cells within the junctional layer are also undergoing apoptosis (Straszewski-Chavez, Abrahams, & Mor, 2005).

The unique subplacenta found in Hystricomorphs consists of fetal tissue and is fully developed during mid-gestation. It is composed of syncytium-encapsulating cytotrophoblast, which is also present in multiple layers at various locations within the subplacenta. By late gestation, the subplacental structure is nearly completely degraded, resembling the junctional zone. The area is still highly vascularized at 55 dpc and individual living cells show immunoreactivity to our cytokeratin- and vimentin-antibodies. Immunohistochemical analyses for both time points indicate that the syncytiotrophoblast in the subplacenta exhibits exclusive immunoreactivity against CK7, whereas cytotrophoblasts solely express cytokeratin19. In the junctional zone at mid gestation, EPTC, syncytial streamer and trophoblastic giant cells exhibit similar immunoreactivity for both

antibodies, while at late gestation the extra-placental trophoblast cells and TGC are similarly immunoreactive to CK7 and CK19. In the chorio-allantoic placenta of 55 dpc, cytokeratin7 is intensely and cytokeratin19 mildly expressed in the fine and coarse syncytium.

Laterally to the subplacenta are chorionic giant cells, accompanied by the parietal endoderm of the yolk sac running alongside. Both structures persist throughout mid and late gestation; however, while fully formed at the earlier time point, there is a notable regression in structural integrity at the later stage. In mouse and rat, the yolk sac is described as fully functional in conduiting nutrients for the first half of the pregnancy but then disappearing in late gestation (Wooding & Burton, 2008). Our material concludes a likewise decline in the activity of this structure, evidenced by diminished cell cohesion and quantity from mid to late gestation.

Large maternal arteries traverse laterally to the subplacenta, which open into the chorio-allantoic placenta and perfuse the fetal tissue with blood. Since our samples lack most of the main placenta at 30.5 dpc, comparison of the 55 dpc to the earlier time point is precluded. Despite its advanced stage, the late-stage placenta shows no indications of cell death. This may be attributed to its delayed attainment of the mature form, typically not achieved until 30 dpc (Carter, Tanswell, Thompson, & Han, 1998), and its subsequent adoption of the role as the primary supporting organ for the embryo until term. It can be clearly seen that maternal blood is separated from the fetal blood by one layer (hemomonochorial) of fine syncytium and flows through the placenta in a labyrinthine manner. This labyrinth is not formed in the coarse syncytiotrophoblast, where only blood vessels are present. Finally, the prominent layer of fetal mesenchyme which developed between the main and subplacenta retains a similar morphology at both time points.

As expected, there is a drastic change in cell composition at the fetal-maternal interface from diestrus/implantation to the later time points in this relatively long pregnancy. Thereby the maternal cell types in myometrial layers remained consistent, whereas the endometrium underwent a complete transformation, transitioning large portions of fibroblast to decidual cells and the disappearance of glands. Fetal cell populations of numerous differentiated cell types now predominate in our examined tissue sections of the fetal-maternal interface. The comparison between mid and late gestation reveals no change in cell types; all those found at the fetal-maternal interface at 30.5 dpc are also present at 55 dpc. Unlike in the comparison between diestrus and implantation, we observe no trend towards proliferation but rather a trend of decreased cell abundance due to necrosis and apoptotic processes towards term.

Interestingly, we observed an infiltration of necrotic vesicles and amorphous masses throughout the entire junctional zone, resulting in a disorganized layer from mid gestation up until term. This is contrary to the distinct necrotic zone, described by Davies, Dempsey, & Amoroso (1961). Another aspect that warrants future attention is the reason for the varied cytokeratin expression in different trophoblast cells.

6.2.1. Comparison of histology with single-cell RNA sequencing experiment

Single-cell RNA sequencing data described in 6.1.1., was also provided for mid (but not late) gestation (30.5 dpc) to obtain insights into the cellular composition. The analyzed tissue samples included the FMI but excluded the chorio-allantoic placenta. Cell populations detected through scRNA-seq coincide with the major cell types identified using histological techniques. Basanta & Stadtmauer (in prep.), identified a significant cluster of maternal decidual cells associated in the UMAP with two subclusters of extra-placental trophoblast cells. Additionally, a cluster of EPTC was identified in the transcriptomes in close proximity to a cytotrophoblast cluster. These three subclusters likely correspond to the syncytial streamer and trophoblast cells invading the junctional zone, and the chorionic giant cells lateral to the subplacenta. Cytotrophoblast cells were identified in high concentrations, and we localize these to the multi-layered cytotrophoblastic subplacenta, as the main placenta was not included in the transcriptomic analysis. Interestingly, syncytiotrophoblast cells were relatively scarce, potentially due to their highly vacuolated nature, or because they are hard to capture in single-cell sequencing.

The transcriptomically identified large clusters of immune cells, particularly macrophages and dendritic cells, probably populate the fetal-maternal interface due to the potential association with necrosis and apoptosis. Smaller clusters of granulocytes and natural killer cells were also detected in the vicinity. Furthermore, the transcriptomic analysis revealed a relatively low abundance of endodermal yolk sac cells and smooth muscle cells compared to other cell populations.

A notable observation is the significant shift in functional cell units compared to earlier gestational stages, as is also described by histology. Several novel cell populations emerge (e.g. decidual cells, trophoblast cells), while others persist, including pericytes, vascular endothelial cells, and the smooth muscle cells of the myometrium. A comparison between the mid and late gestation time points is not possible as the transcriptomic data does not include samples at 55 dpc.

6.3. Comparison of maternal and fetal histology of guinea pig and mouse

Mice are considered model species in biomedical experimental research, meaning that many of the insights are considered transferable to humans. While true for many traits and organ systems, when it comes to reproduction and pregnancy, we recognize (as mentioned in the introduction) a variety of differences between mice and humans. These include the interhemal space of the placenta, length of pregnancy, uterine shape, number of offspring and more (Aguilera, et al., 2022). This prompts critical evaluation of the mouse model's suitability for human traits. Comparison with guinea pigs reveals greater resemblance to human reproductive traits, suggesting potential advantages for drawing conclusions on this topic (Mess, 2007). Here, we briefly compare our findings in guinea pig to mouse, to discern similarities and differences in reproductive tissue morphology in these two rodent species. This analysis utilizes the book “The Guide to Investigation of Mouse Pregnancy” (2014) alongside our findings on guinea pigs.

Examining the diestrus mouse uterus, we note the same basic structure observed in guinea pigs. The uterine lumen is surrounded by endometrium, pervaded by tubular glands. Croy et al. (2014) also categorize the endometrium into superficial and deep stroma and mention the similarity to the human endometrium. The inner myometrium comprises circumferential muscle bundles, while the outer myometrium consists of longitudinal bundles, both separated by a vascular layer.

Contrary to the interstitial implantation in guinea pig, the blastocyst's attachment in mouse occurs as the uterine lumen envelops the embryo, developing within a narrow endometrial cleft. It adheres between 5 and 6 dpc and invades the anti-mesometrial side of the endometrium akin to the guinea pig. The cellular composition during diestrus and implantation mirrors our findings in guinea pigs. During mouse implantation occurs an accumulation of erythrocytes attributed to increased vascularization, a phenomenon also anticipated in guinea pigs (Canizo, Zhao, & Petropoulos, 2024) but not corroborated in our study as the implantation sites were not present in our samples.

Mouse and guinea pig gestations encompass different portions of embryonal/fetal development, with guinea pig feti born in precocial state, and mouse feti in very early developmental stage (altricial). Thus, relative pregnancy stages (mid, late) are not directly comparable. Since we assume that uterine progression must undergo specific transformations during the pregnancy, in part independently of the developmental stage of the embryo/fetus, we will compare the stages relative to the pregnancy lengths in both species, with some caution.

It is essential to note that while comparisons regarding gestation will be made, it's acknowledged that the chosen time points are not directly homologous between both species. Given the short gestation period in mice (19-21 days), the selected mid gestational time point for comparing the guinea pigs FMI is around 10 dpc. Out of the four chosen time points, the most significant shift in cell populations at the mouse fetal-maternal interface, occurs towards mid gestation. At this point, the myometrium is thinly stretched, consistent with the observation in guinea pig. In mouse, a lymphoid aggregate forms on the mesometrial side between the myometrium and decidua, which is not observable (or mentioned in literature) in the guinea pig. The newly differentiated decidua basalis in mouse occupies the majority of the maternal tissue space, permeated by blood vessels and invasive extra-placental trophoblast cells. In contrast, in guinea pigs, the latter is restricted to the so-called junctional zone, which refers to a part of the actual interface, not as in mouse, a region of the main placenta. Maternal decidual giant cells are absent in mouse gestational tissue and present in guinea pig. The placental side of the interface itself is in mice a well-defined layer devoid of necrotic or apoptotic masses. It comprises a continuous layer of trophoblastic giant cells, similar to the chorionic giant cells in guinea pigs, encircling the outer edge of the chorio-allantoic placenta. Additionally, the spongiotrophoblast, where glycogen trophoblasts also appear, is part of the junctional part of the placenta. Although distinct layers, both serve as a junction between decidua and placental structures (Wooding & Burton, 2008). Notably, the giant cell layer in guinea pigs is discontinuous and ends between the junctional zone and subplacenta. This discrepancy constitutes a significant difference between mice and guinea pigs, as mice lack a subplacenta. In mice, the chorio-allantoic placenta consists partially of junctional zone. Despite both species exhibiting a labyrinthine placental structure, the interhemal space in mice is three-layered. They display hemotrichorial placentation (in contrast to hemomonochorial placentation in guinea pigs), with two layers of syncytium and one layer of trophoblastic giant cells between maternal blood space and fetal endothelium. The giant cells surrounding the blood space differentiate into two subpopulations. Additionally, the mouse placenta is partly enveloped by a parietal yolk sac placenta, serving as a nutrient source for the first half of pregnancy before rupturing and then dissolving prior to term.

The selected late gestational time point for comparing guinea pig to mouse is around day 19 after copulation, with the understanding that these late time points are also not homologous between both species. Generally, the cell composition does not vary between mid and late gestation in mice. Similarly to guinea pigs, we can observe a regression of maternal cell abundance. The layers are reduced in proportion compared to the fetal tissue. Most of the chorio-allantoic placenta in mice consists of labyrinth at this stage, merged with the junctional zone. In late gestation, the

mouse placenta becomes functionally hemodichorial, as the layer of TGCs becomes perforated, leaving two layers of separation between maternal blood space and fetal endothelium.

Overall, there are fundamental similarities in maternal cell types between mouse and guinea pig, like epithelial and endothelial cells, fibroblasts and pericytes, especially in early phases of pregnancy. As the pregnancy progresses and the endometrium transforms, the tissue structures begin to diverge more strongly between the two species. The main difference in cell composition of the decidua basalis in mice is the presence of EPTC and the absence of decidual giant cells. Also absent are the necrotic and apoptotic zones in mice, which may be ascribed to the much longer gestation of the guinea pig. The developing fetal tissue, especially the distribution and morphology of trophoblastic cells, shows most divergence between both species, which underscores the necessity for nuanced comparative analyses.

7. Conclusion

Even if we observe a similar cell pattern in one particular gestational stage among mammals, it can differ entirely in another stage. The endometrium, serving as the critical tissue enabling placental development, may exhibit relative stability across eutherian species. In contrast, the placenta is highly variable across different mammalian taxa. This variation encompasses multiple dimensions, including the arrangement of layers, degree of invasiveness, diversity of cell types, and overall morphology. To comprehensively understand the complexity of the evolution and function of the placenta, it is imperative to delve into comparative studies of a wide range of non-model species and examine the foundational tissue involved in placental development. The guinea pig study addressed here is a contribution to such comparative knowledge, adding a rodent species with very different reproductive characteristics than a conventional rodent model species, such as mouse or rat.

The morphological changes in the fetal-maternal interface of the guinea pig during gestation, as shown here by mid and late gestational phase, have significant implications for understanding the dynamic interactions between maternal and fetal tissues. The intricate network of decidual cells, trophoblasts, and necrotic decidua in the guinea pig junctional zone underscores the complexity of the fetal-maternal interface during this critical period. The questions to be answered in the future are what distinct role the subplacenta has, why it undergoes apoptosis from day 45 (Davies, Dempsey, & Amoroso, 1961) at least 15 days prior to parturition, and what processes affect this apoptosis. By day 55 after copulation, the main chorio-allantoic placenta apparently adopts the entire function of supporting the fetus.

It is important to acknowledge the limitations of our study, including the insufficient sample amount for diestrus, implantation and mid gestation. The samples for these stages were each obtained from one individual guinea pig, which does not take potential variability between individuals into account. Furthermore, many antibodies available have only been tested positive on model species, mice in this case. In consequence, we observed multiple non-binding antibodies, such as Anti-Oxytocin-neurophysin 1, Anti-SDF1 and one of the Vimentin antibodies (goat polyclonal). In the cases of Anti-CD45 and Anti-CD11b, the low intensity of the signal, caused by either erroneous concentration or low binding affinity of antibodies, did not provide a distinct result. Some of the questions remaining unanswered are where myometrium borders on decidua basalis, how to distinguish decidual giant cells from the remaining decidual cells, or why the gland size decreases in implantation stage. For further non-histological research, the underlying

mechanisms and functions of the broad necrotic junctional zone offer a promising area for investigation.

In summary, the guinea pig uterus undergoes substantial changes during gestation, involving dynamic shifts in tissue composition, vascularization, and cellular activities at the fetal-maternal interface. The comparison between non-pregnant and pregnant states provides insights into the adaptations apparently necessary for successful pregnancy in this species. Our findings underscore the complexity of the fetal-maternal interface and shed light on several key aspects that contribute to our understanding of uterine development and fetal-maternal interactions in guinea pigs.

8. References

Aguilera, N., Salas-Pérez, F., Ortíz, M., Álvarez, D., Echiburú, B., & Maliqueo, M. (2022). Rodent models in placental research. Implications for fetal origins of adult disease. *Animal Reproduction*, 1-19. doi:https://doi.org/10.1590/1984-3143-AR2021-0134

Al-Saffar, F., & Al-Ebbadi, H. (2019). Histomorphological and Histochemical Study of the Uterus of the Adult Guinea Pigs (Cavia Porcellus). *Indian Journal of Science and Technology*, 12(46). doi:10.17485/ijst/2019/v12i46/148620

Andersen, M., Alstrup, A., Duvald, C., Mikkelsen, E., Vendelbo, M., Ovesen, P., & Pedersen, M. (2018). Animal Models of Fetal Medicine and Obstetrics. In I. Bartholomew, & editor, *Experimental Animal Models of Human Diseases* (S. 343-347). London: IntechOpen. doi:http://dx.doi.org/10.5772/intechopen.74038.

Arendt, D., Musser, J., Baker, C., Bergman, A., Cepko, C., Erwin, D., . . . Wagner, G. (2016). The origin and evolution of cell types. *Nature Reviews*, 17:744-757.

Basanta, S., & Stadtmauer, D. (in prep.). Comparative single cell analysis receals complex patterns of cell type and cell signaling innovations at the fetal-maternal interface. Unpublished work. Department of Theoretical Biology, University of Vienna.

Brosens, J., de Souza, N., & Barker, F. (1995). Uterine junctional zone: function and disease. *Lancet*, 346: 558-560.

Canizo, J., Zhao, C., & Petropoulos, S. (2024). The Guinea Pig: A New Model for Human Preimplantation Development. *bioRxiv*, 1-93.

Carter, A., & Enders, A. (2004). Comparative aspects of trophoblast development and placentation. *Reproductive Biology and Endocrinology*, 2:46. doi:10.1186/1477-7827-2-46

Carter, A., Tanswell, B., Thompson, K., & Han, V. (1998). Immunohistochemical Identification of Epithelial and Mesenchymal Cell Types in the Chorioallantoic and Yolk Sac Placentae of the Guinea-pig. *Placenta 19*, 489-500.

Chavan, A., & Wagner, G. (2016). The fetal-maternal interface of the nine-banded armadillo: endothelial cells of maternal sinus are partially replaced by trophoblast. *Zoological Letters*, 2:11. doi:10.1186/s40851-016-0048-1

Croy, A., Yamada, A., DeMayo, F., & Adamson, S. (2014). *The Guide to Investigation of Mouse Pregnancy.* USA: Academic Press. doi:978-0-12-394445-0

Davies, J., Dempsey, E., & Amoroso, E. (1961). The Subplacenta Of The Guinea-Pig: Development, Histology And Histochemistry. *Journal of Anatomy, Vol.95*, 457-473.

Emera, D., Romero, R., & Wagner, G. (2011). The evolution of menstruation: A new model for genetic assimilation. *BioEssays*, 34:26-35.

Enders, A. (1965). A comparative study on the fine structure of the trophoblast in several hemochorial placentas. *American Journal of Anatomy, 116*, 29-68.

Enders, A., & Schlafke, S. (1969). Cytologial aspects of trophoblast-uterine interaction in early implantation. *American Journal of Anatomy, Vol.125, I.1*, 1-29. doi:https://doi.org/10.1002/aja.1001250102

IHC World, LLC. (24. October 2023). Von https://www.ihcworld.com/_protocols/special_stains/masson_trichrome.htm abgerufen

IHC World, LLC. (24. October 2023). Von https://www.ihcworld.com/_protocols/special_stains/pas.htm abgerufen

Kirkwood, P., Gibson, D., Smith, J., Wilson-Kanamouri, J., Kelepouri, O., Esnal-Zufiaurre, A., . . . Saunders, P. (2021). Single-cell RNA sequencing redefines the mesenchymal cell landscape of mouse endometrium. *Faseb Journal*, 35:e21285 . doi:https://doi.org/10.1096/fj.202002123R

Kliman, H., Sammar, M., Grimpel, Y., Lynch, S., Milano, K., Pick, E., . . . Gonen, R. (2012). Placental Protein 13 and Decidual Zones of Necrosis: An Immunologic Diversion That May be Linked to Preeclampsia. *Reproductive Sciences 19(1)*, 16-30. doi:DOI: 10.1177/1933719111424445

Mess, A. (2007). The Guinea Pig Placenta: Model of Placental Growth Dynamics. *Placenta 28*, 812-815.

Mess, A., Zaki, N., Kadyrov, M., Korr, H., & Kaufmann, P. (2007). Caviomorph Placentation as a Model for Trophoblast Invasion. *Placenta 28*, 1234-1238.

Richani, K., Romero, R., Soto, E., Nien, J., Cushenberry, E., Kim, Y., . . . Kim, C. (2007). Genetic Origin and Proportion of Basal Plate Surface-Lining Cells in Normal and Abnormal Pregnancies. *Hum Pathol.*, 38(2): 269-275.

Soncin, F., Natale, D., & Parast, M. (2015). Signaling pathways in mouse and human trophoblast differentiation: a comparative review. *Cell Mol Life Sci*, 72(7):1291-1302. doi:doi:10.1007/s00018-014-1794-x

Straszewski-Chavez, S., Abrahams, V., & Mor, G. (2005). The Role of Apoptosis in the Regulation of Trophoblast Survival and Differentiation during Pregnancy. *Endocrine Reviews 26(7)*, 877-897. doi:10.1210/er.2005-0003

Wildman, D., Chen, C., Erez, O., Grossman, L., Goodman, M., & Romero, R. (2006). Evolution of the mammalian placenta revealed by phylogenetic analysis. *PNAS*, 103:9:3203-3208. doi:https://doi.org/10.1073/pnas.0511344103

Wilson, J. (1927). On the Question of the Interpretation of the Structural Features of the Early Blastocyst of the Guinea-Pig. *Journal of Anatomy*, vol.LXII:Part 3.

Wooding, P., & Burton, G. (2008). *Comparative Placentation - Structure, Functions and Evolution.* Berlin: Springer.